SPATIAL REPRESENTATION IN THE MAMMALIAN BRAIN

FIELD-TO-FIELD VARIABILITY OF GRID CELLS

Michaela Poth (nee Pröll)
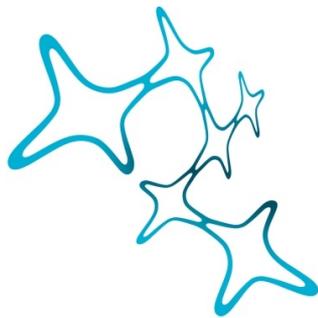
Graduate School of Systemic Neurosciences

LMU Munich
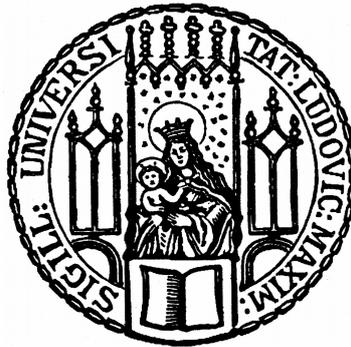
Dissertation at the
Graduate School of Systemic Neurosciences
Ludwig-Maximilians-Universität München

April, 2020

OVERVIEW

_____

Cognitive maps are neuronal representations of the world. These are required for animals to efficiently navigate. Grid cells in the medial entorhinal cortex are heavily involved in forming a basis of such cognitive maps. They are active at multiple locations of the environment and these locations form an imaginary hexagonal grid tessellating the explored space.

While firing fields in two-dimensional environments are regularly spaced, grid cells seem to respond different for movements along a linear track, a quasi one-dimensional environment. On such a linear track, they show multiple firing fields which are not periodically arranged and whose shape and position change when the running direction is reversed. In both, one- and two-dimensional environments, the firing rates of a grid cell vary widely from field to field.

In this thesis, we investigate possible reasons that lead to the field-to-field variability of grid cell recordings in 1d and 2d.

The research is presented in the from of two articles; one accepted paper and one manuscript. Both articles are included as single chapters preceded by a brief summary, each. The following sections give a short overview of the thesis.

The introduction provides a recapitulation of animals' spatial behavior leading to the assumption that they have a cognitive map. We review a few of the most important observations about spatial representations in the brain. To this end, we describe the anatomical organisation of the hippocampal formation, a brain region containing most of the cells involved in spatial navigation

and representation. A literature review about place and grid cells follows.

In the published paper, the field-to-field variability of the grid-cell activity along a linear track is studied (chapter 2). For each running direction, firing fields turn out to be compatible with a slice through a two-dimensional (2D) hexagonal pattern. We show that a single hexagonal pattern can explain the one-dimensional data if a translational shift is allowed at the movement turning point.

In the manuscript, a possible role of the burst activity for the field-to-field variability in two-dimensional environments is investigated (chapter 3). We show that burst activity plays no role for this variability or for rate remapping. Furthermore, we demonstrate that theta-phase coding is preserved but we do not observe differences between the first and second half of the theta cycle.

Finally, our results are discussed and future experiments and analysis are proposed.

CONTENTS

ACRONYMS

CA   Cornu Ammonis

DG   dentate gyrus

MEC   medial entorhinal cortex

LEC   lateral entorhinal cortex

PrS   presubiculum

PaS   parasubiculum

ISI   interspike interval

INTRODUCTION

1.1 SPACE

What is space? Philosophers, mathematicians and physicists have been debating about the nature and essence of space for thousands of years. The earliest reports go back to the ancient Greeks.

In mathematics, space came a long way. It started with the abstraction of physical space in Euclid's elements and went on with Rene Descartes' introduction of the Cartesian coordinates via analytic geometry. Then, Gauss coined the term non-Euclidean geometry and referred it to his own theory which is called "hyperbolic geometry" nowadays. For the non-Euclidean geometry Euclid's fifth axiom, the parallel postulate, has to be replaced by its negation. Finally, the notation of topological space came up. This definition relies only upon set theory and builds the most general notion of a mathematical space that allows for the definition of concepts such as continuity [107]. Similarly, classical Physics was located in a three-dimensional space until Einstein came up with a continuum of space and time [75]. At the time of the ancient Greeks, philosophers started debating the essence of space. Plato was convinced that space exists always, cannot be destroyed and gives a place in which all things come to be. Much later, Leibniz and Newton had a great debate about the definition of space. Leibniz was convinced that space just exists as the

relation between objects and cannot exist if these objects do not exist. In contrast, Newton took the view that space is the frame of reference, in which all objects can move. This frame of reference can exist even without objects inside [15]. In "Critique of the Pure Reason" Kant claimed, that space allows us to comprehend experience and is not a substance, an entity in itself or a learned experience. It is empirically real and not an illusion [57].

In the following, we define space in a very pragmatic way and think of it as a physical arena, where we live in and navigate through [89]. The abilities of animals to move in space and to navigate are fascinating. The arctic tern, for example, lives in the arctic for 14 weeks per year and only a bit longer in the antarctic. For the rest of the year, they fly from one home to the other one. This means they travel around 22.000 miles per year and find their way without a hitch. Pigeons are famous for their innate homing ability, too. They can return from distances of up to 1.000 miles and therefore do not need landmarks [58]. Hence, they have been well-established as messenger pigeons since at least 550 BC [66]. They mainly use the sun or the magnetic field for navigation. Interestingly, if they are released at the same location multiple times, they return home by the same route very rarely [58]. In contrast, desert ants, for example, do not primarily rely on external cues. While traveling a random path, they estimate their position relative to the starting point. Regarding this as a geometrical problem, they add up the vectors for each part of the journey from the origin and take the inverse vector for the navigation back. This is called path integration or dead reckoning. Hereby, the vestibular organs play an important role, as they detect the acceleration. This information is then combined with motor efference, optic flow and in some animals echolocation or

magnetoreception to allow the mammalian brain to calculate the actual position [36, 79, 97]. It has been shown, that desert ants forage and return afterwards hundreds of meters by counting steps, even through unfamiliar and identical looking environments. Mammals do not count steps but rather integrate their head-direction and speed. With the support of somatosensory information and motor efference copy the mammalian brain is able to compute the position of the animal [36, 79]. However, counting steps or adding up similar internal signals is a very noisy process, especially for long-range navigation. To correct these errors, other signals have to be used, e.g., desert ants can navigate to a goal with the help of landmarks. Indeed, in cluttered environments this can override the path-integration system [16, 25, 104, 126]. Thereby, the relative position of the goal to the landmarks can be called a map. If such a map is stored in the brain, it is referred to as a cognitive map.

Ecological observations about spatial navigation through the physical space have been discussed for centuries. However, one question has hardly been addressed: Where is the space or the spatial map in the brain?

In the next section we will focus on this question. Hereby, we concentrate on mammals - specifically on rats, as they have been studied predominantly.

1.2 THE NEURONAL REPRESENTATION OF SPACE − THE HIPPOCAMPAL FORMATION

Arantius gave the first description of the hippocampus in 1587 [69]. He collated the protrusion on the floor of the temporal horn to a "sea horse" (hippocampus) but alternated between this term

and "silkworm". Duvernoy, who illustrated the hippocampus first in 1729, hesitated between the two terms "hippocampus" and "silkworm", too [69]. To complicate matters, the hippocampus was named differently over the years. Winslow suggested the term "ram's horn" in 1732, De Garengeot preferred "Cornu Ammonis" and Diemerbroeck (1672) introduced the term "pes hippocampi" [69]. These days, the structure is just called "hippocampus" and the term "Cornu Ammonis" is only preserved in the names of the hippocampal subfields CA1-CA4.

In general, the hippocampal formation is a compound structure in the medial temporal lobe composed of the dentate gyrus, the hippocampus proper and the subiculum (Figure 1a). The mammalian hippocampal formation is located in the medial temporal lobe of the brain and is involved in spatial navigation and memory. This has been observed in several anatomical, physiological and lesion experiments [37, 76, 82, 89, 97]. Superficial layers of the entorhinal cortex are the main origin of the perforant pathway targeting hippocampus, while the hippocampal back projection terminates in deeper layers of the cortical laminar structure (Figure 1b).

Throughout the hippocampal formation, background oscillations were found. These oscillations have a frequency of about 8 Hz and are called "theta rhythm". They were observed in the extracellular field potential [8, 17, 21] as well as in the subthreshold potentials of individual neurons [6, 31, 56, 106]. Many neurons seem to oscillate slightly faster than the extracellular field potential. This leads to a phenomenon named "phase precession". It refers to the fact that the spikes tend to occur at successively earlier phases relative to the ongoing theta cycle over the course of a few theta periods [48, 90]. Phase precession in the hippocampal
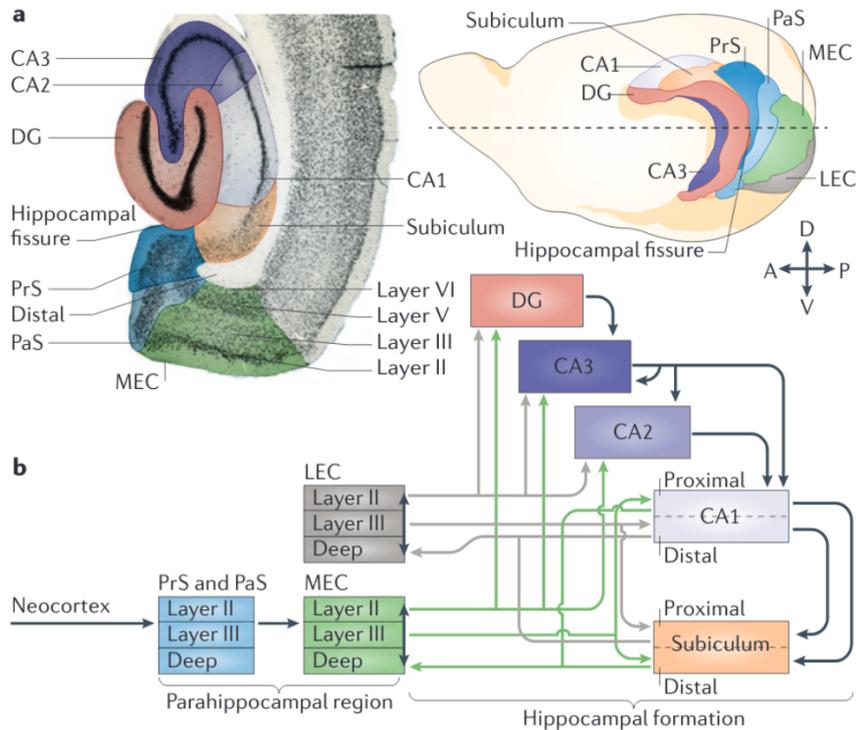
Figure 1: Hippocampal and parahippocampal formation.

a) A nissl-stained horizontal cross section of the hippocampal and parahippocampal formation (left panel) and a mid-sagittal view (right panel). The following abbreviations are used: the dentate gyrus (DG), the Cornu Ammonis (CA), the medial entorhinal cortex (MEC), the lateral entorhinal cortex (LEC), the presubiculum (PrS) and the parasubiculum (PaS). b) The standard connectivity model is depicted. The entorhinal layers are reciprocally connected. This is shown by the double-headed arrows. These connections are colored in green and paralleled by a grey route but start and end in the LEC. Reprinted with the permission from [84]

formation was studied in spatially modulated cells, place cells and grid cells, which will be introduced in the next sections.

Initially, the hippocampus was thought to be a part of the olfactory system. In the 19th and early 20th centuries, it was noticed that across species the size of the olfactory bulb and the size of the parahippocampal gyrus are correlated [40]. In 1900, there was a first hint that the hippocampal formation is involved in memory formation and recall. At this time, the Russian neurologist Vladimir Bekhterev described the significant memory deficits of two patients. The autopsy unveiled softening of hippocampal and adjacent cortical tissue [14].

In the 1950s, a first fundamental observation was made. Scoville and Milner reported in 1957 that human lesions of the temporal lobe – specifically the hippocampus, led to a loss of recent episodic memory. However, the ability to retrieve old memories was not impaired. Thus, patients like Henry Gustav Molaison (H.M.) suffered an anterograde amnesia because the transfer of information from the short-term to the long-term memory was not possible any more [108]. From this time on, many clinical and functional-imaging studies provided evidence that the hippocampal system is crucial for declarative memory [20, 28, 34, 111]. Specifically, it was found that the hippocamapal system is more important for episodic memory, e.g., remembering autobiographical events, than for semantic memory [124, 125]. In 1971, a second fundamental observation was made. O'Keefe and Dostrovsky found cells in rat's hippocampus which are highly active whenever the animal is at a certain place in the environment and remain silent elsewhere – the so-called place cells [87, 88]. These cells were considered as the neural substrate of a "spatial cognitive map" straightaway. This means, they were

seen as an allocentric internal representation of space supporting navigation, self-location and spatial memory [89, 123].

Thus, the hippocampal formation is involved in both, spatial navigation and episodic memory. Moreover, it has been reported that the hippocampal formation represents spatial and non-spatial variables as time [72], odors [33] or sounds [1, 9].

1.3 PLACE CELLS

Hippocampal place cells fire whenever the animal is within a certain place in the environment and remain silent elsewhere [88]. The area of activity within the environment is called place field (Figure 2a-c). The population of place cells forms a complete representation of the recording environment because the centers of the place fields are spread over the entire arena (Figure 2d). Furthermore, the size of place fields increases along the dorsoventral axis and ranges from 20 cm to 10 m or more [18]. However, it is still under discussion whether the size increases gradually or in discrete steps [115]. Place cells with more than one field were observed, especially in larger environments [67, 92]. Thus, a few place fields can be used to reconstruct the animal's position precisely [129].

The firing activity of place cells is stable in familiar environments even over a period of several months [121]. It has been suggested that the spatial activity of place cells is innate, as place cells appear just a few days after the pubs open their eyes [64, 128].

Furthermore, dissimilarities between environments are reflected in place cells. In 1987, Muller and Kubie studied how populations of place cells respond to changes of the recording
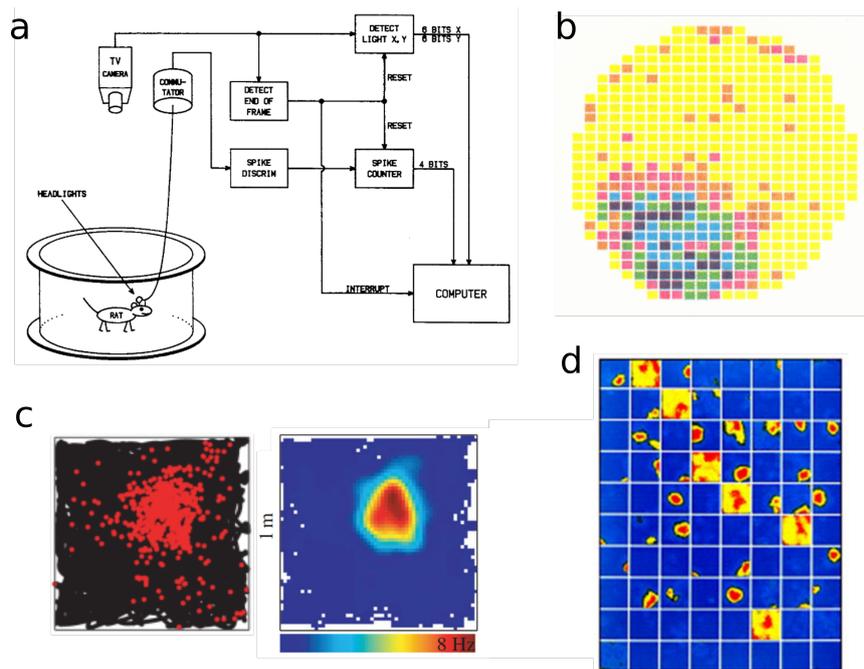
Figure 2: Place cells.

a) Place cell recording setup of a freely moving rat in a circular recording environment. The animal's X and Y coordinates are tracked via an LED on its head, registering the locations where the cell fires a spike. b) Firing rate map. On a pixel-by-pixel basis, the number of spikes is normalized by the time spend in each pixel. a and b are reprinted with permission from [86]. c) The left panel depicts a place cell recording with the animals trajectory (black) and the spikes (red dots). Typically, the activity of a place cell is visualised by a smoothed firing rate map (right panel). Areas with lower activity are blue, areas of high activity are red. Reprinted with permission from [55]. d) A population of place cells can represent all locations within the environment by its firing rate code. When the animal explores an environment, a sequence of place cells conveys information about its location. The centers of the place fields are spread all over the environment. Reprinted with permission from [83].

environment [85]. They reported that the presentation of two different enclosure shapes (circle and square) leads to a reorganization of the hippocampal map. This phenomenon is known as remapping. According to further experimental results, three different kinds of remapping in place cells can be distinguished: global, partial and rate remapping. When place cells are recorded in two environments that differed in multiple features as shape, color and location of the recording box, global remapping was observed. Thereby, in each environment only a small subset of the place cell population is active. The two subsets that are active in the different environments are random samples from the entire place cell population [5, 121]. Some cells are active in both environments but the locations of their firing fields are not related [5, 67, 68, 85, 96, 128]. Partial remapping is usually observed when just a few – usually non-metric or contextual – cues of the recording environment are changed, e.g., color and odor. This affects only a subgroup of place cells while the others remain stable [7]. Rate remapping is reported for small changes of the environment, e.g., the location of the arena remains but the color or the shape of the enclosure is varied. Then, the position of the place fields is stable across recordings but the mean firing rate varies from field to field up to an order of magnitude [68]. So, it was shown that the hippocampus conveys information about the position of the animal and specific cues of the environment simultaneously. This has also been shown for various memory tasks [3, 4, 39].

1.4   HEAD DIRECTION CELLS

Head-direction cells are active when the animal's head points in a specific direction, the preferred firing direction of the cell. The firing rate decreases when the animal turns its head away from the preferred direction [118]. These cells were found in a number of brain regions including the entorhinal cortex [44], postsubiculum [119] and the thalamus [80, 117]. The preferred firing direction remains stable if the animal is recorded multiple times in the same, familiar environment. Allocentric, mostly visual cues seem to influence the initial head-direction preference. Head-direction cells depend on the vestibular system [118]. Especially the semicircular canals of the inner ear are essential, since they signal rotations of the animal's head [130]. Based on theoretical and lesion works, it is assumed that head-direction cells in the hippocampal formation provide input to grid cells.

1.5   GRID CELLS

Fyhn et al. reported in 2004 that neurons in the most dorsolateral part of the MEC show multiple firing fields [43]. These firing fields are spaced regularly and the pattern resembles a hexagonal lattice (Figure 3a), which justifies the name: grid cells [49]. The spatial firing pattern of a grid cell can be characterized by the following properties (Figure 3b):

- `grid scale or spatial period`: the firing peak-to-peak distance between two neighboring firing fields.

- `grid spatial phase`: the two-dimensional spatial offset between the firing fields and a reference point.

- `grid orientation`: the angle between one of the grid axis and a reference direction.

The scale and orientation of neighboring cells, e.g., cells which are simultaneously recorded, is similar. However, the phases are uniformly distributed, thus, a few grid cells can cover the recording environment [49].
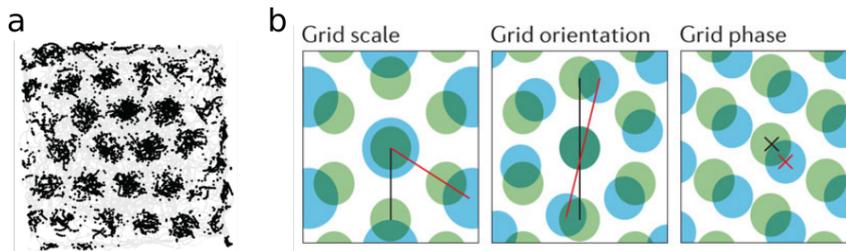
Figure 3: Basic grid cell properties.

    a) The firing patterns of grid cells can be characterised in terms of their geometrical configurations. b) If the triangular arrangement of firing fields is regular, the spatial firing patterns of grid cells can be characterized by the following properties: the firing peak-to-peak distance between two neighboring firing fields (grid scale; left panel), the angle between one of the grid axis and a reference direction (grid orientation; middle panel) and the two-dimensional spatial offset between the firing fields (grid phase; right panel). Reprinted with permission from [84].

Along the dorsoventral axis the spatial period and the field size of grid cells increase monotonically. Thereby, the period ranges from 20 cm up to several meters [19, 42, 49]. However, this increase is not continuous. Barry et al. (2007) observed that the grid scale varied in discrete steps [13]. Theoretical and experimental work showed that the ratio between two subsequent grid scales is a constant number, about 1.4 to 1.7 [62, 74, 112, 113, 127]. Furthermore, Stensola et al. (2012) found that grid-cell

activity is organized in only a few modules. Within a module, grid patterns differ by a global phase offset but show a similar scale, orientation and theta-frequency modulation. However, these properties vary significantly across modules. They sampled about half of the dorsoventral MEC and see four to five modules per animal. This gives a first hint that the total number of grid modules in the MEC is about ten. These modules also have a large overlap in anatomical space, spanning multiple cortical layers and extending to pre- and parasubiculum [113]. Furthermore, the firing rates vary from field to field up to an order of magnitude when the animal is freely foraging in an arena. These seem to be stable across time and sessions within the same setting [32, 54].

Usually, grid cell activity is unaffected by the size or aspect ratio of a familiar arena. If a squared environment is rescaled abruptly, e.g., stretching along one or two axis, grid patterns adapt correspondingly [13] or reorganize their fields entirely [105]. The deformations are consistent within but not across modules.

In 2015, Krupic et al. demonstrated that grid cells do not necessarily show the regular structure but tend to align to the walls of the arena. This alignment seems to be persevered even after the rotation of the arena [62, 114]. When grid cells are recorded in environments with more complex boundary shapes, e.g., trapezoidal enclosures [62, 63], the triangular symmetry of grid-cell firing was destroyed. In hairpin mazes, the hexagonality is entirely gone [29]. If an animal is running along a linear track, grid cells show multiple firing fields. However, the firing pattern is not as periodic as in 2d environments and the firing rates vary widely from field to field. The firing rate profiles for movements in each running direction are consistent with slices through a 2d hexagonal pattern [131]. Thus, the animal could interpret

the linear track as a part of the 2d environment and supports the hypothesis that the hexagonal patterns provide a universal metric used for spatial navigation. In contrast, various studies observe differences between the two running directions [19, 29, 47, 70, 93].

The firing pattern of a grid cell is stable when the cell is recorded in the same familiar environment several times. However, if an animal is exploring the same box but the color or the shape of the enclosure is changed, the grid pattern does not move whereas the rates specific to each firing field change [30]. This is known as "rate remapping". Further, when smaller changes to the environment are introduced, e.g., recording in a different box but in the same room, the patterns shift. Thereby, the shifts of grid cells from the same module (cells that are recorded from the same electrode and featuring a similar firing pattern) are coherent [41]. Similarly, larger changes of the environment, e.g., recording in two identical boxes in different rooms, lead to a translational shift and a rotation of the grid pattern. Hereby, the relative phase relationship remains constant within modules, too [41]. Nonmetric context changes such as different odors can result in a purely translational shift [73]. In these cases, size and spacing of the grid fields do not change across environments. By contrast, in novel environments, e.g., an arena the animal experiences the first time, the firing pattern of a grid cell expands and is less regular than in familiar environments. This attenuates with experience over several recording days [12].

Grid cells encode information also on shorter time scales than the firing rates reflect, i.e., phase precession [48, 55, 99, 100] and burst firing [65]. Bursts are defined as at least two spikes separated by an interspike interval (ISI) of less than 8 ms or 10 ms and can

have discharge rates up to 300 Hz [65]. Burst firing decreases gradually along the dorsal-ventral axis [11]. For other brain regions, theoretical studies have been suggested that bursting can provide unique benefits [71]. It has been proposed that bursts can increase the reliability when information is transferred [60, 71]. Thus, the probability of a response in postsynaptic neurons is higher for bursts and especially for longer bursts [27, 110]. Further, Kepecs and Lisman (2003) assumed that sensory stimuli could be encoded by the burst length [59]. Later, this has been revealed in many neural systems [10, 38, 61]. Bursting has also been demonstrated to correspond with spatial coding. In the hippocampus [35, 81, 85, 91] and the subiculum [109], the animal's position can be estimated more precisely when bursts and not single spikes are used. In grid cells, bursts are correlated with spatial information and are associated with a high signal-to-noise ratio [11].

There are grid cells which are not only modulated by the animal's position but also by idiothetic signals such as head direction. Due to this, they are named conjunctive cells [103]. They might play an important role in updating the internal position estimate [76] and are mainly observed in layer III [44, 103].

2

GRID-CELL ACTIVITY ON LINEAR TRACKS

2.1 SUMMARY

When rodents explore a 2d environment, the firing fields of each grid cell form a periodic hexagonal pattern. For movements along a linear track, highly irregular firing fields were observed. These are not periodically arranged and the width of the fields as well as the peak firing rates vary widely. For each running direction, the firing fields correspond to a cut through a highly regular 2d hexagonal pattern. This provides first evidence that 1d environments could be interpreted as a part of 2d environments. Thus, grid cells might provide a universal metric for spatial navigation. In contrast, it was observed that the position of firing fields and peak firing rates vary between both running directions.

We study how the direction-dependent activity can be embedded in 2d firing patterns. We will show that one lattice is not enough to explain the data recorded on a linear track. Both running directions can only be explained if a translational shift of the hexagonal pattern is allowed at the movement turning point.

2.2   REFERENCE

This work was done under the supervision of Stefan Häusler and Andreas Herz; M.P., S.H., and A.V.M.H. designed research; M.P., S.H., and A.V.M.H. performed research; M.P. analyzed data; M.P., S.H., and A.V.M.H. wrote the paper. Parts of the work were presented as a poster at the Bernstein Conference on Computational Neuroscience 2016 and 2017. The paper has been accepted in *Journal of Neuroscience* with the following reference:

M. Pröll, S. Häusler, and A.V.M. Herz. "Grid-cell activity on linear tracks indicates purely translational remapping of 2D firing patterns at movement turning points." In: *Journal of Neuroscience* (2018), accepted June 24, 2018.

Systems/Circuits

Grid-Cell Activity on Linear Tracks Indicates Purely Translational Remapping of 2D Firing Patterns at Movement Turning Points

Michaela Pröll, Stefan Häusler, and Andreas V.M. Herz

Bernstein Center for Computational Neuroscience Munich and Faculty of Biology, Ludwig-Maximilians-Universität München, 82152 Planegg-Martinsried, Germany

Grid cells in rodent medial entorhinal cortex are thought to play a critical role for spatial navigation. When the animal is freely moving in an open arena the firing fields of each grid cell tend to form a hexagonal lattice spanning the environment. For movements along a linear track the cells seem to respond differently. They show multiple firing fields that are not periodically arranged and whose shape and position change when the running direction is reversed. In addition, peak firing rates vary widely from field to field. Measured along one running direction only, firing fields are, however, compatible with a slice through a two-dimensional (2D) hexagonal pattern. It is an open question, whether this is also true if leftward and rightward runs are jointly considered. By analyzing data from 15 male Long–Evans rats, we show that a single hexagonal firing pattern explains the linear-track data if translational shifts of the pattern are allowed at the movement turning points. A rotation or scaling of the grid is not required. The agreement is further improved if the peak firing rates of the underlying 2D grid fields can vary from field to field, as suggested by recent studies. These findings have direct consequences for experiments using linear tracks in virtual reality.

Key words: grid cells; linear track; medial entorhinal cortex; remapping; spatial navigation

---

Significance Statement

Various types of neurons support spatial navigation. Their response properties are often studied in reduced settings and might change when the animal can freely explore its environment. Grid cells in rodents, for example, exhibit seemingly irregular firing fields when animal movement is restricted to a linear track but highly regular patterns in two-dimensional (2D) arenas. We show that linear-track responses of a cell for both leftward and rightward running directions can be explained as cuts through a single hexagonal pattern if translational remapping is allowed at movement turning points; neither rotations nor scale transformations are needed. These results provide a basis to quantify grid-cell activity in 1D virtual reality and could help to detect and categorize grid cells without experiments in 2D environments.

Introduction

When a rodent explores an open arena, grid cells in its medial entorhinal cortex discharge in spatial firing patterns that resemble hexagonal lattices (Hafting et al., 2005). The spatial scales of

these lattices approximate a geometric series so that discrete grid-cell modules arise (Stensola et al., 2012). The grid patterns of cells within the same module are aligned and differ only by a global phase offset. When the animal moves along a linear track, grid cells seem to respond differently. Their spike activity is still spatially modulated but no longer periodic. In addition, the peak firing rates of a given grid cell differ strongly from field to field (Lipton et al., 2007; Brun et al., 2008; Derdikman et al., 2009; Gupta et al., 2014). Firing fields recorded along one running direction are, however, compatible with a slice through a two-dimensional (2D) hexagonal lattice (Yoon et al., 2016). This suggests that the animal interprets the one-dimensional (1D) linear track as part of a two-dimensional environment, and supports the view that grid cells provide a universal metric for spatial navigation.

This view is challenged by the observation that grid fields measured along a linear track vary between left-to-right and right-to-left runs (Lipton et al., 2007; Brun et al., 2008; Derdikman et al., 2009; Gupta et al., 2014; Pérez-Escobar et al., 2016), suggesting that the one-dimensional activity patterns of a grid cell cannot correspond to a single slice through the same fixed two-dimensional lattice. Instead, translations, rotations, or even scale transformations might be needed to explain the experimental data. Because the study of Yoon et al. (2016) was restricted to runs in one direction, it could not address this important aspect.

To analyze how direction-dependent 1D activity patterns are embedded in 2D lattices, we investigated four different scenarios. First, grid-cell responses could, in principle, correspond to slices through the same one lattice (OL) for both running directions (Fig. 1A). Given the experimental evidence (see Brun et al., 2008), this is an unlikely scenario. Nevertheless, it provides a helpful null hypothesis. Next, we considered two scenarios motivated by remapping experiments in 2D environments. Larger changes (e.g., moving the animal to a new room) can cause a translation and rotation, while smaller changes to the environment, such as changing the enclosure but not the room (Fyhn et al., 2007) or nonmetric context changes (Marozzi et al., 2015) typically lead to a pure translational shift of the grid pattern within the enclosure. Taking such remapping experiments into account, we hypothesized that when considering two opposite running directions, the underlying 2D patterns could be identical except of a translational (S) shift or an additional rotation ($S+R$), as shown in Figure 1, B and C. Note that rotations by multiples of 60° are equivalent to pure shifts (S). Finally, the two hexagonal lattices might also be scaled differently ($S+R+Sc$), as depicted in Figure 1D.

Here, we show that a joint hexagonal firing pattern explains the linear-track data for both running directions as soon as a translational shift (S) is allowed. Importantly, added rotations ($S+R$) or additional scalings ($S+R+Sc$) of the grid are not needed. The agreement between measured data and the model framework improves further if the firing rates of the underlying 2D grid field can vary from field to field, as has been suggested recently (Diehl et al., 2017; Dunn et al., 2017; Ismakov et al., 2017).

These findings reveal that the hexagonal firing-field structure of grid cells can persist even in quasi one-dimensional environments. This does not imply that the same is true in enclosures with strong asymmetries, as is evident from the seemingly irregular arrangement of grid fields in trapezoidal arenas (Krupic et al., 2015). Our results do, however, provide a basis to quantify and interpret the grid-cell activity of animals running on linear tracks in virtual reality (Domnisoru et al., 2013; Schmidt-Hieber and Häusser, 2013) and could help to detect and categorize grid cells without experiments in two-dimensional arenas.

Materials and Methods

Data. We analyzed spike-train data from Brun et al. (2008). These authors recorded grid cells from 15 male Long–Evans rats on a linear track that was 18 m long and extended over three successive rooms. The track passed through two doorways located 9.5 and 12 m from the west end of the track; the starting position was located at the east end. To avoid artifacts associated with the doors, we focused our analysis on data from within the largest room. Therefore, and to avoid contamination by sharp-wave-related firing, spikes that were recorded <40 cm from the west and east walls of this room were excluded from further analysis, resulting in the same effective track length of 8.7 m for all recording sessions.

Grid cell selection. Although all recorded cells were classified as grid cells in 2D, not all showed spontaneous activity and sufficiently spatially
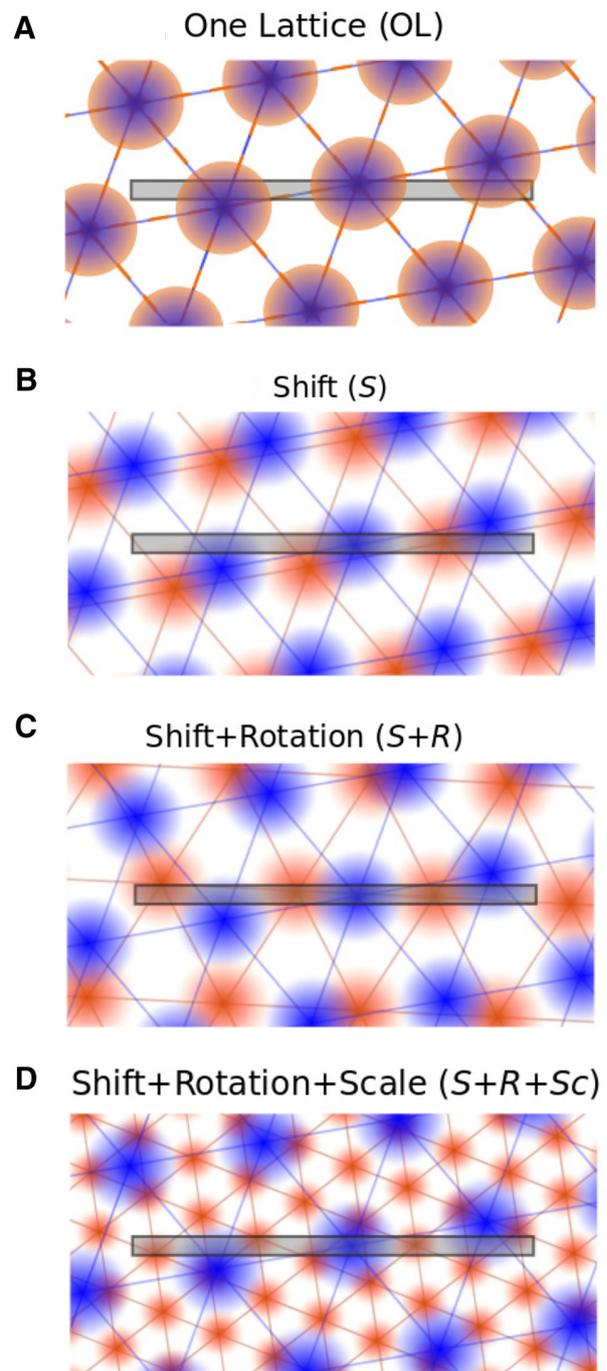
Figure 1. Four scenarios. *A*, One Lattice (OL): a joint hexagonal firing pattern underlies grid-cell activity on both left-to-right runs (orange firing fields) and right-to-left runs (blue firing fields) along a linear track, which is shown as a gray horizontal bar in all subpanels. *B*, Shift (*S*): compared with *A*, the joint hexagonal firing patterns may be shifted differently for both running directions. Notice that within this scenario a rotation of the lattice by multiples of 60° can be described by a pure shift. *C*, Shift+Rotation (*S+R*): apart from translational shifts (*S*) rotations are now allowed, too. *D*, Shift+Rotation+Scale (*S+R+Sc*): in addition to shifts (*S*) and rotations (*R*), the scales (*Sc*) of the underlying hexagonal grids may vary between the two running directions.

modulated firing along the linear track. We therefore excluded cells if they did not spike at all for >70 cm in a row or if the mean-to-maximum firing rate ratio was >0.2 in the analyzed room. From the data on 143 cells provided to us, 67 cells were left.

Firing rate. We divided the track into bins of 1 cm. Similar to Brun et al. (2008), we calculated rate maps using spatial smoothing with a Gaussian kernel. The rate at each position is as follows:

$$\lambda(x) = \frac{\sum\limits_{i=1}^{n} g\left(\dfrac{s_i - x}{h}\right)}{\displaystyle\int\limits_{0}^{T}\left(\dfrac{y(t)_i - x}{h}\right)},$$

with the mean firing rate $\lambda(x)$ for bin x and a Gaussian kernel, g, with a smoothing factor of 3.5 cm; n is the number of spikes, s_i is the position of the ith spike, h is the spatial smoothing factor, T is the length of session, and $y(t)$ is the position of the rat at time t.

Error measurement. To determine the quality of the fit, we use the mean squared error between the firing rate along the linear track and the fit, normalized by the firing rate, as follows:

$$\text{error} = \frac{\sum(\text{firingrate}(t) - \text{fit}(t))^2}{\sum(\text{firingrate}(t))^2}.$$

Consequently, the error for each recording is the sum of the error for left-to-right and right-to-left runs divided by 2.

Slices. To test the hypothesis that firing rates along a linear track can be interpreted as one-dimensional slices through a two-dimensional hexagonal lattice, we assumed periodic von Mises tuning curves (Herz et al., 2017) in 2D. The 1D slices can then be parametrized with the following parameters: μ, period of the hexagonal lattice; σ, width of the firing fields of the lattice; $\hat{f}$, peak firing rate for the grid; (x, y), starting point; and φ, angle of the grid rotation, confined (without loss of generality) to the interval [0°, 30°].

x, y, and φ describe the position of the stripes in the lattice. The parameters μ, σ, and $\hat{f}$ determine the hexagonal lattice. So, the firing rate in a point in the hexagonal lattice is given by the following:

$$R(x, y, \sigma, \mu, \hat{f}) = \frac{\hat{f}}{\exp\left(\dfrac{4.5\sigma}{\mu}\right)}$$

$$* \left[\exp\left[\frac{\sigma}{\mu} * \left(\cos\left(\frac{4\pi}{\sqrt{3}\mu} * \cos\left(\frac{\pi}{6}\right) * x - \sin\left(\frac{\pi}{6}\right) * y\right)\right) \right.\right.$$

$$+ \left(\cos\left(\frac{4\pi}{\sqrt{3}\mu} * \cos\left(\frac{\pi}{6}\right) * x + \sin\left(\frac{\pi}{6}\right) * y\right)\right)$$

$$\left.\left.+ \left(\cos\left(\frac{4\pi}{\sqrt{3}\mu} * \cos\left(\frac{\pi}{2}\right) * x + \sin\left(\frac{\pi}{2}\right) * y\right)\right) + 1.5\right)\right] - 1$$

Apart from the lattice transformations considered here—purely translational shifts (S), added rotations ($S+R$), as well as additional scaling transformations ($S+R+Sc$)—one could in principle also study pure R or Sc operations and $R+Sc$ combinations. For those mappings, however, one has to specify an "anchor point" (i.e., the fixed point of the R and/or Sc operation). As this involves an arbitrary choice, we do not systematically study such scenarios.

Fitting procedure. To minimize the error between the slice model and the measured firing rates, we first used an extensive search procedure at an intermediate parameter resolution (brute force search). Grid-field spacing and field size could vary between 80% of the smallest values and 120% of the largest values reported by Brun et al. (2008). No restriction was applied to the rotation angles; because of the sixfold and mirror symmetries of the hexagonal grid, only angles between 0° and 30° had to be considered. The search intervals were divided into 10–50 bins depending on their size and the number of different parameters explored in one run.

This procedure resulted in sets of approximate parameters for the preliminary error minima. We then took the parameters for the 15 smallest errors with a pairwise different lattice period, μ. These sets were used as initial conditions for Powell's method (scipy package) to find local minima. To avoid solutions where one running direction would be fitted perfectly and the other only poorly, the errors of both running directions were not allowed to differ more than three times the SD of the errors between left and right runs in the model $S+R+Sc$. To find a robust minimum, we first varied the parameters of the local minima slightly and used them again as initial conditions for Powell's method. This procedure was repeated 500 times. To further improve the search process, we then picked the eight fits with the smallest error and used them as initial conditions for another run of Powell's method. This procedure was repeated 100 times. The slice with the smallest error is called best fit. To study the robustness of the fitting procedure, we doubled the number of parameters in the first step for three cells used as test cases and repeated the second step of the minimization process as described before. The results were stable.

Random rotations. We tested the influence of rotations by rotating the best fits of each recording 1000 times randomly. The resulting mean errors are given in the Results.

Experimental design and statistical analysis. We reanalyzed data originally recorded by Brun et al. (2008) and refer the reader to that publication for details on the experimental design. All our analyses were performed in Python (RRID:SCR_008394). Specific statistical tests used are stated throughout the text. The Wilcoxon rank-sum test as well as the linear regression were taken from Python scipy.stats (RRID:SCR_008058) and the Rayleigh test and the circular–circular correlation from Matlab circstats (RRID: SCR_001622). To show that the shifts do not have a preferred length, we used the Wilcoxon rank-sum test for samples drawn from a uniform distribution and the distribution of the length of the shifts. We repeated the test 1000 times with different samples and give the mean p value in the text.

Shift along the track for the model shift. We analyzed the offsets in the slices of right-to-left and left-to-right runs for simultaneously recorded cells from the same module. The offsets were optimized as described above (see Fitting procedure); spacing as well as the rotation had to be the same for all cells from the same module.

Bootstrapping. We bootstrapped the firing rates of each direction of a cell by using sampling with replacement. We randomly drew a single run. The selection process was repeated until there were as many runs as in the original session. We then calculated the firing rates and the error between the original and the bootstrapped firing rates.

Results

When rodents move along a linear track in one direction, their grid-cell activity profiles are consistent with slices through two-dimensional hexagonal firing patterns (Yoon et al., 2016). This study did, however, not address the key question of how the 2D lattices for movements in opposite directions are related to each other. The lattices could be identical or differ in some or all grid parameters, as shown by the four scenarios sketched in Figure 1, with important consequences for the principles underlying grid-cell coding.

To distinguish between these alternatives, we reanalyzed grid-cell data recorded by Brun et al. (2008) (Materials and Methods: Data and grid-cell selection) and tested for the four scenarios shown in Figure 1. For each model, we searched for slices through 2D hexagonal lattices that optimally fit the measured 1D firing fields on the linear track. The fit quality was assessed by the normalized mean squared error between the fit and the measured data (Materials and Methods, Error measurement), as illustrated in Figure 2. To find optimal lattices, we first applied an exhaustive search procedure at an intermediate parameter resolution, followed by an iterative scheme based on Powell's method (Materials and Methods, Fitting procedure).
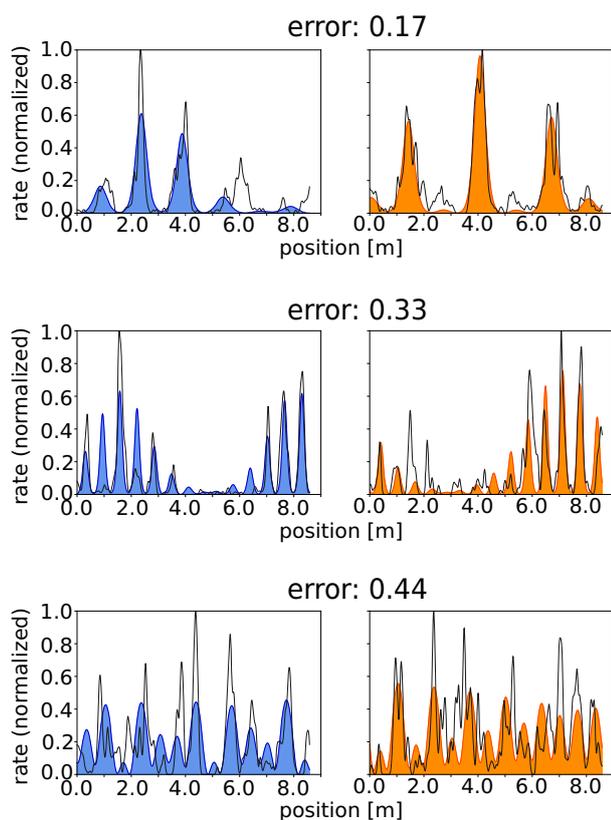
Figure 2. Three examples of best fits of the firing rate along a linear track: left/right panels show the measured firing rates along the track (black lines) and the firing rates predicted from cuts through two-dimensional hexagonal patterns (blue/orange) for left-to-right/right-to-left runs.

A single hexagonal lattice cannot explain the linear-track data

The mean error of $S+R+Sc$ models averaged over all grid cells and animals is 0.24 (Fig. 3A). This value serves as a reference for the goodness of fit for the other three scenarios and can largely be explained by measurement noise and potential deviations from a prefect grid (see below). The mean errors for the other three scenarios $S+R$, S, and OL are 0.28, 0.33, and 0.49. The large drop in fit quality from S to OL suggests that the OL model does not capture the one-dimensional firing-field data. The somewhat higher errors of the $S+R$ and S models compared with the $S+R+Sc$ model presumably can be attributed to distorted grid patterns or measurement noise that differs for both running directions. The significance of these errors is evaluated in the next section.

To understand the model differences cell by cell, we performed a regression analysis (Fig. 3B). This is applied to the errors of the best fits in the scenarios $S+R+Sc/S+R$, $S+R/S$, and S/OL. The large slope of 0.96 and the small intercept of 0.05 ($r = 0.87$, $p = 6.36\mathrm{e}{-}22$, SE $= 0.07$) in the relation between the $S+R+Sc$ and $S+R$ models (Fig. 3B, left) implies that for each cell the fit quality deteriorates only marginally when the grid scales are identical for left-to-right and right-to-left runs. Similarly, if the rotational degree of freedom is removed when switching from the $S+R$ to S model (Fig. 3B, second panel), the slope is still large (0.97) and the intercept is still small (0.06; $r = 0.91$, $p = 3.64\mathrm{e}{-}26$, SE $= 0.06$). Once grid translations are no longer allowed (Fig. 3B, third panel), the slope approaches a small value (0.24) with large intercept (0.41; $r = 0.22$, $p = 0.17$, SE $= 0.13$). As shown in Figure 3C,

there is no systematic relation between the fit quality and the relative lattice rotation for right-to-left versus left-to-right runs. However, there are numerous low-error solutions in the $S+R$ scenario so that a restriction to shifts results only in a small increase of the mean error (0.33 instead of 0.28). This increase is not the result of a small impact of rotations on the fit quality. In fact, random rotations of the best fits lead to a large mean error (1.34; see Materials and Methods, Random rotations). Furthermore, the shifts for the S model are random in direction (Rayleigh test: $p = 0.20$, $n = 67$) and length (Wilcoxon rank-sum test: $p = 0.17$, $n = 67$; see Materials and Methods) and not animal specific (Fig. 3D). The same applies to the shift along the track even for cells from the same module that were simultaneously recorded (Fig. 3E). The distribution of the angles between the shifts of one session does not differ from the angular distribution of the surrogate data (circular–circular distribution: $p = 0.02$; see Materials and Methods, Shift along the track, statistical analysis). Thus, the difference in the mean error for the S and the OL models cannot be explained by a uniform field shift of all the grid fields of one animal. We expect uniform shifts within a single module (Yoon et al., 2013) but do not have a sufficient amount of data to test this hypothesis.

Translational remapping alone is sufficient to explain grid cell activity

In general, the more model parameters are optimized, the lower the model error. Thus, the small error of the $S+R+Sc$ model could be due to the large number of 12 parameters compared with the $S+R$ and S models with 10 and 9 parameters, respectively. The decrease in the error reflects either an improvement in the description of the underlying data structure or overfitting of noise.

To address this issue, we generated surrogate data with partially identical grid parameters for both running directions. We constructed three datasets by combining firing patterns from specific left-to-right and right-to-left runs from different animals. The first dataset consists of randomly chosen firing patterns for each direction so that their optimal grid parameters are independent. We refer to this dataset as D_{S+R+Sc} (Fig. 4A). The second and third datasets consist of combinations of firing patterns that share the same scale parameters, or the same scale and orientation parameters for the grids of both running directions, respectively. We denote these datasets as D_{S+R} (Fig. 4B) and D_S (Fig. 4C).

$S+R+Sc$ models optimized for each of the three datasets D_{S+R+Sc}, D_{S+R}, and D_S have approximately the same quality as for the original data with mean errors of ~0.24 for all three datasets. The error distributions are also not statistically different [Wilcoxon rank-sum test: p (D_{S+R+Sc}) = 0.95, p (D_{S+R}) = 0.87, p (D_S) = 0.93, $n = 67$].

$S+R$ models optimized for the D_{S+R} dataset have nearly the same mean error (0.29) as for the original data (0.28), and the corresponding error distributions (Fig. 4B) are not statistically different (Wilcoxon rank-sum test: $p = 0.70$, $n = 67$). Thus, we observe a similar performance difference between the $S+R+Sc$ and the $S+R$ models for the D_{S+R} dataset compared with the original data. For the D_{S+R}, this difference cannot be attributed to different scale parameters of the grids for both running directions but rather suggests overfitting.

Likewise, the errors of S models optimized for the D_S dataset have the same mean value (0.33) as for the original data (0.33; Fig. 4C), and the corresponding error distributions are not statistically different (Wilcoxon rank-sum test: $p = 0.76$, $n = 60$). Again, we observe a similar performance difference between $S+R+Sc$
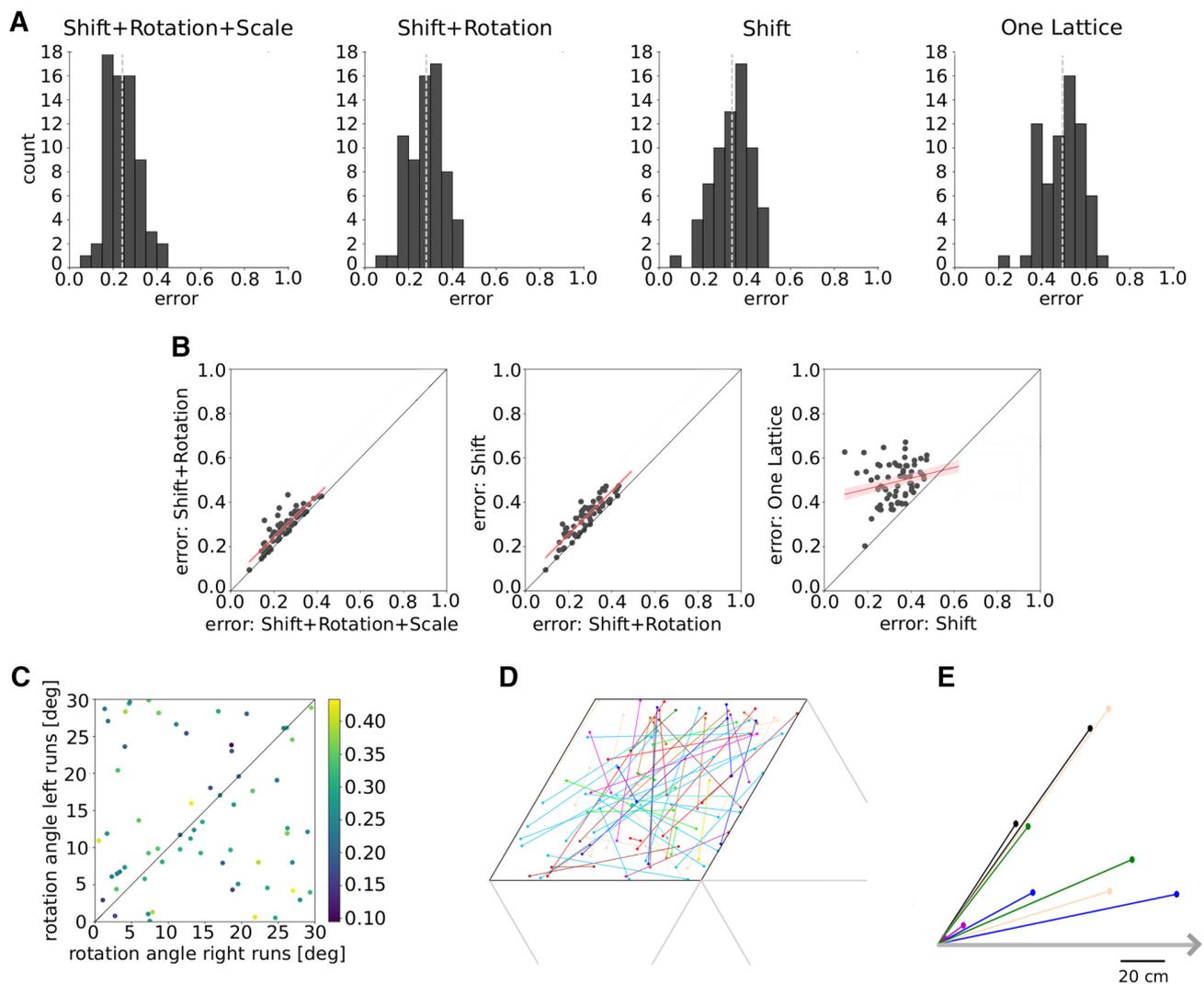
Figure 3. *A*, Error distributions for the best fits in the four model scenarios: Shift+Rotation+Scale, Shift+Rotation, Shift and One Lattice. The light gray dotted lines denote the mean of each distribution. *B*, Cell-by-cell analysis. Each dot in the scatter plots represents the best fits for one grid cell and the two scenarios indicated by the axis labels. Red lines indicate linear regressions with confidence intervals in light red. *C*, Rotation angles of the two-dimensional grid for left and right runs (Shift+Rotation). The color indicates the fit error. *D*, The two offsets (filled circles) in a pair of parallel slices (model *S*), within a rhomboidal unit cell of the unit lattice. Cells from the same animal have the same color. *E*, Offsets in a pair of parallel slices (model *S*) relative to the left end of the track, which is shown as a gray arrow. Simultaneously recorded cells from the same module have the same color.

and S models for the D_S dataset and the original data. For the D_S dataset, this difference cannot be attributed to different parameters of the grids for both running directions but again points to overfitting. These results indicate that the S model is sufficient to describe the structure of the firing rate patterns given that the noise on the surrogate data and the original data is the same.

To show that hexagonal lattices indeed capture the structure of the firing rate patterns for runs in opposite directions, we compared the performance of $S+R$ models for the D_{S+R+Sc} dataset and the original data. A difference in the mean errors indicates that the scale parameters of the hexagonal lattices for both running directions depend on each other. We measured a mean error of 0.35 for the D_{S+R+Sc} dataset (and 0.28 for the original dataset). Furthermore, the error distributions of the original data and the D_{S+R+Sc} dataset are significantly different (Wilcoxon rank-sum test: $p = 3.91\text{e-}06$, $n = 67$), as illustrated in Figure 4A.

Similarly, a difference in the mean errors of S models for the D_{S+R} dataset and the original data indicates that the rotation

parameters of the hexagonal lattices of both running directions depend on each other. Here, we assume that the $S+R$ model is sufficient to describe the structure of the original data (as shown above) so that the scale parameters of grids for both running directions are the same for the original data and the D_{S+R} dataset. We measured a mean error of 0.47 for the D_{S+R} dataset (and 0.33 for the original dataset), and the error distributions of the original data and the D_{S+R} dataset are significantly different (Wilcoxon rank-sum test: $p = 2.10\text{e-}08$, $n = 67$), as illustrated in Figure 4B.

Overall, these findings imply that the parameters of grids for left-to-right and right-to-left runs have a specific relationship that is sufficiently captured by the S model when compared with the $S+R$ and $S+R+Sc$ model.

Data suggest only small deviations from perfect grids
To estimate the impact of measurement noise on the results, we bootstrapped the firing rates (see Material and Methods, Bootstrapping) 100 times in each running direction and calculated the errors as before. For the $S+R+Sc$ model, the average error be-
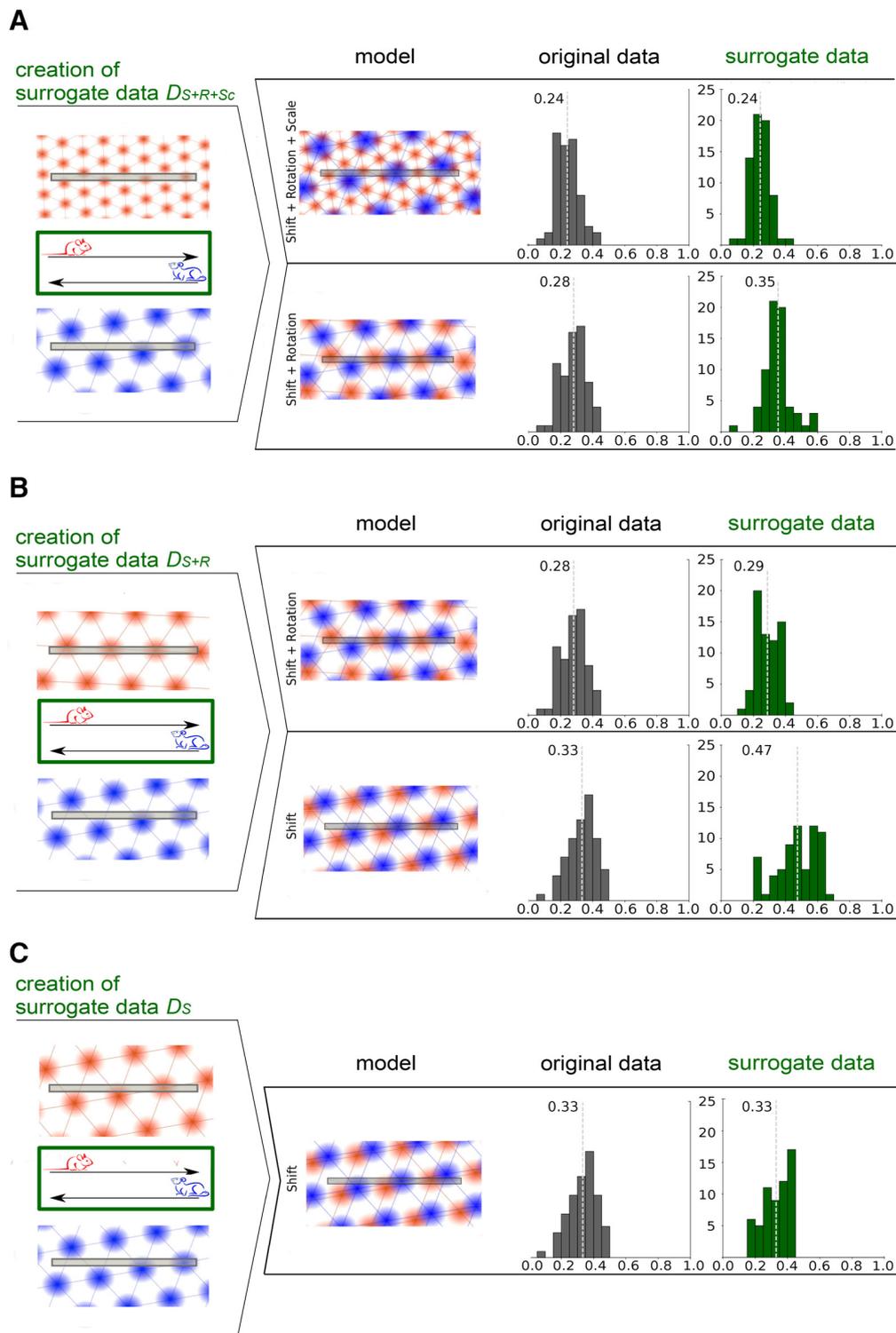
Figure 4. Error distribution for surrogate data for the scenarios Shift + Rotation and Shift. Each light gray dotted line indicates the mean of the error distribution. **A**, Creation of surrogate data D_{S+R+Sc} for the model Shift and Rotation by combining left-to-right and right-to-left runs from different animals and fitting these for the models Shift + Rotation + Scale and Shift + Rotation. **B**, Creation of surrogate data D_{S+R} for the model Shift were fitted for Shift + Rotation and Shift. Error distributions of the original (gray) and surrogate (green) data. **C**, Creation of surrogate data D_S by combining left-to-right and right-to-left runs with similar grid spacings and rotations from different animals and fitting these for the models Shift.

tween the bootstrapped samples and the original firing rate profiles is 0.12, with an SD of 0.08. As the mean error of the $S+R+Sc$ model is 0.24 (Fig. 3A), approximately half of this value can be explained by measurement noise.

Recent work has shown that the firing rate maxima of grid cells in two-dimensional environments vary from field to field (Diehl et al., 2017; Dunn et al., 2017; Ismakov et al., 2017). To take this structural variability of the data into account, we fitted
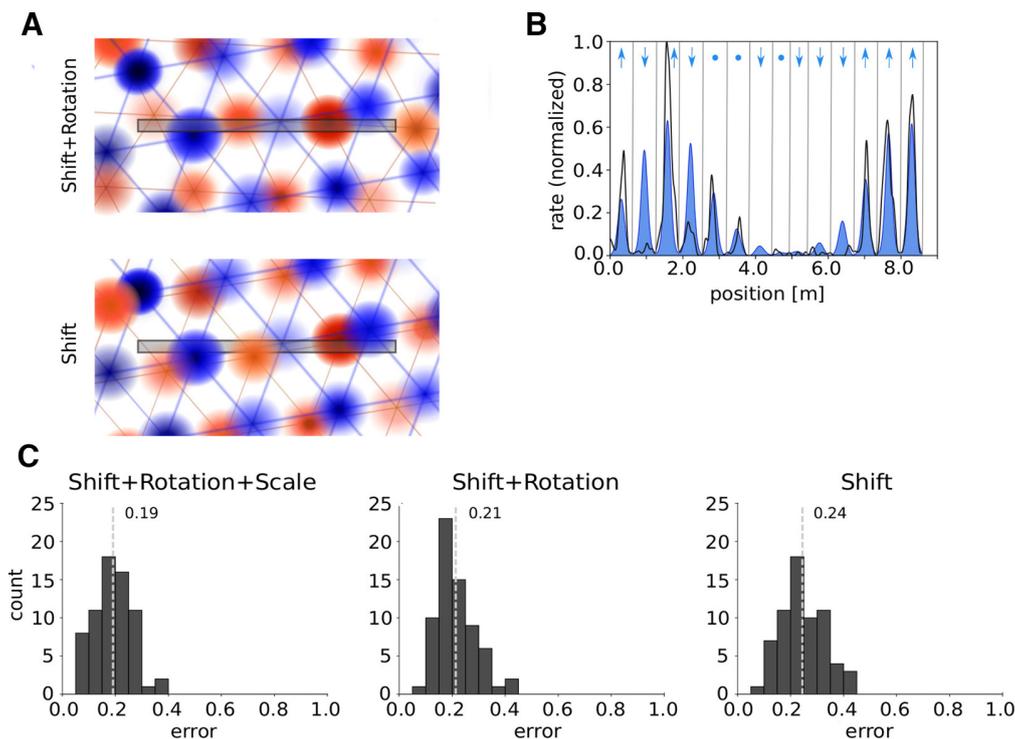
Figure 5. *A*, Visualization of the cases Shift and Shift + Rotation if peak firing rates differ for each firing field. *B*, Visualization of the approach. The normalized firing rate for the left-to-right runs is shown in black, and the best fit in blue. The vertical lines define single bins that extend from one minimum of the fit to the next one. The arrows indicate whether the peak firing rate of the particular firing field should be higher or lower, or should remain constant. *C*, Error distribution for the cases Shift + Rotation + Scale, Shift + Rotation and Shift. The light gray dotted lines indicate the mean error of each error distribution.

the measured data as before and subsequently optimized the size of the local peak firing rates by minimizing the mean squared error for each firing field (Fig. 5B). This approach was chosen to avoid overfitting that results from optimizing all parameters simultaneously. All models improved their performance compared with the original scenarios ($S+R+Sc$: mean error, 0.19; improvement, 0.05 or 21%; Wilcoxon rank-sum test: $p = 1.81e$-03, $n = 67$; $S+R$: mean error, 0.21; improvement, 0.07 or 25%; Wilcoxon rank-sum test: $p = 3.12e$-08, $n = 67$; S: mean error, 0.24; improvement, 0.09 or 27%; Wilcoxon rank-sum test: $p = 2.63e$-08, $n = 67$). The model S benefits most from the variability of the peak firing rates in 2D in absolute and relative terms.

The improvement of the performance of the model S cannot be explained by overfitting. To show this, we estimated the effect of overfitting using bootstrapped firing rates. Optimizing the size of the local peak firing rates for the bootstrapped data leads to a mean error improvement of 0.04 compared with the true error for the sampling distribution (mean error, 0.24). As the performance of the S models with and without varying peak heights differs by 0.08, it is highly unlikely to be due to overfitting alone ($p = 2.07e$-3). Grid cells exhibit strikingly periodic firing patterns in rectangular or circular arenas that seem to break down in polarized environments (Krupic et al., 2015). We hypothesize that the residual errors of the S models might be ascribed to such displacements of the firing rate peaks. In fact, a displacement of only 15 cm explains the residual mean error of 0.12 (average field size, 86 cm).

Discussion

Grid cells have been hypothesized to provide a universal metric for space (Hafting et al., 2005), based on their highly regular

firing fields in open arenas. This raises the question whether the seemingly irregular arrangement of grid fields along linear tracks is compatible with a hexagonal lattice structure.

Indeed, as shown by Yoon et al. (2016), the firing fields from runs in one direction are compatible with slices through two-dimensional hexagonal firing fields. This study did, however, not address the relation between firing fields of left-to-right versus right-to-left runs. To relate the lattices underlying both running directions, we analyzed four models that decreased stepwise in complexity. We started with a scenario including shifts, rotations, and scale transformations and went to one where a single lattice directly governs grid-cell firing in the two opposite movement directions. Only in this last scenario could the firing activity be interpreted as a slice through a single fixed lattice. Our analysis shows, however, that this is not the case. Instead, the lattice needs to be shifted when the animal turns around for the next lap—but rotations or scale transformations of the grid are not required. Similar conclusions hold for an extended scenario that takes the field-to-field variability of 2D firing rate maxima (Diehl et al., 2017; Dunn et al., 2017; Ismakov et al., 2017) into account. Together, these findings imply that there is significant remapping at the movement turning points and that this remapping respects the geometric properties that define a single grid-cell module (same orientation, same spatial scale, but variable spatial phases).

A purely translational shift seems to be plausible because the animals run through a cue-rich, familiar environment. Scale transformations are expected only if the environment is familiar to the animal in one direction and is novel in the other direction (Barry et al., 2012), and rotations are only expected for larger changes of the environment (Fyhn et al., 2007).

Nonmetric cues could be perceived differently while running in different directions, and that could lead to a translational realignment of the grid pattern (Marozzi et al., 2015). Note in this context that grid-cell responses on circular 1D tracks (Yoganarasimha et al., 2011; Newman et al., 2014) seem to be consistent with circular slices through 2D lattices, while remapped responses on a circular track may result from shifts in the phase of the circular slice (Neunuebel et al., 2013).

When the animal turns around at the ends of the track, the two-dimensional lattices of each grid cell may rotate by 180° due to the input of head-direction cells. Such a rotation can also be described by a pure shift within the S scenario. At the population level, the relation between the shifts of different grid cells depends on whether the grids rotate or stay the same. Imagine, for example, two cells with the same spacing and partly overlapping firing fields. Under a 180° rotation, the temporal order of their activation is identical in the two running directions—and reversed if there is no rotation. This observation shows how to detect 180° rotations on linear tracks. As the available dataset contained only a handful of simultaneously recorded cell pairs from the same module, we could not investigate this issue, which remains an open question for future studies.

The investigated dataset (Brun et al., 2008) does not contain grid-cell data from open arenas so that we could not compare the grid parameters estimated from linear-track data with those from movements in open arenas. An alternative dataset from Pérez-Escobar et al. (2016) provides data recorded on a linear track and in 2D environments, but the linear track is too short to unambiguously reveal an underlying hexagonal pattern. Note also that the number of simultaneously recorded cells in the study by Brun et al. (2008) is rather low so that phenomena at the population level could not be studied. Regardless of these limitations, our results provide a basis to quantify and interpret the grid-cell activity of animals running on linear tracks in virtual reality (Domnisoru et al., 2013; Schmidt-Hieber and Häusser, 2013). Once validated with data recorded from animals moving on linear tracks and in open arenas, this approach will help to detect and to characterize grid cells in one-dimensional virtual reality without the need of additional recordings in real two-dimensional environments.

References

Barry C, Ginzberg LL, O'Keefe J, Burgess N (2012) Grid cell firing patterns signal environmental novelty by expansion. Proc Natl Acad Sci U S A 109:17687–17692. CrossRef Medline

Brun VH, Solstad T, Kjelstrup KB, Fyhn M, Witter MP, Moser EI, Moser MB (2008) Progressive increase in grid scale from dorsal to ventral medial entorhinal cortex. Hippocampus 18:1200–1212. CrossRef Medline

Derdikman D, Whitlock JR, Tsao A, Fyhn M, Hafting T, Moser MB, Moser EI (2009) Fragmentation of grid cell maps in a multicompartment environment. Nat Neurosci 12:1325–1332. CrossRef Medline

Diehl GW, Hon OJ, Leutgeb S, Leutgeb JK (2017) Grid and nongrid cells in medial entorhinal cortex represent spatial location and environmental features with complementary coding schemes. Neuron 94:83–92.e6. CrossRef Medline

Domnisoru C, Kinkhabwala AA, Tank DW (2013) Membrane potential dynamics of grid cells. Nature 495:199–204. CrossRef Medline

Dunn B, Wennberg D, Huang Z, Roudi Y (2017) Grid cells show field-to-field variability and this explains the aperiodic response of inhibitory interneurons. arXiv 1701.04893 [q-bio.NC].

Fyhn M, Hafting T, Treves A, Moser MB, Moser EI (2007) Hippocampal remapping and grid realignment in entorhinal cortex. Nature 446:190–194. CrossRef Medline

Gupta K, Beer NJ, Keller LA, Hasselmo ME (2014) Medial entorhinal grid cells and head direction cells rotate with a T-maze more often during less recently experienced rotations. Cereb Cortex 24:1630–1644. CrossRef Medline

Hafting T, Fyhn M, Molden S, Moser MB, Moser EI (2005) Microstructure of a spatial map in the entorhinal cortex. Nature 436:801–806. CrossRef Medline

Herz AV, Mathis A, Stemmler M (2017) Periodic population codes: from a single circular variable to higher dimensions, multiple nested scales, and conceptual spaces. Curr Opin Neurobiol 46:99–108. CrossRef Medline

Ismakov R, Barak O, Jeffery K, Derdikman D (2017) Grid cells encode local positional information. Curr Biol 27:2337–2343.e3. CrossRef Medline

Krupic J, Bauza M, Burton S, Barry C, O'Keefe J (2015) Grid cell symmetry is shaped by environmental geometry. Nature 518:232–235. CrossRef Medline

Lipton PA, White JA, Eichenbaum H (2007) Disambiguation of overlapping experiences by neurons in the medial entorhinal cortex. J Neurosci 27:5787–5795. CrossRef Medline

Marozzi E, Ginzberg LL, Alenda A, Jeffery KJ (2015) Purely translational realignment in grid cell firing patterns following nonmetric context change. Cereb Cortex 25:4619–4627. CrossRef Medline

Neunuebel JP, Yoganarasimha D, Rao G, Knierim JJ (2013) Conflicts between local and global spatial frameworks dissociate neural representations of the lateral and medial entorhinal cortex. J Neurosci 33:9246–9258. CrossRef Medline

Newman EL, Climer JR, Hasselmo ME (2014) Grid cell spatial tuning reduced following systemic muscarinic receptor blockade. Hippocampus 24:643–655. CrossRef Medline

Pérez-Escobar JA, Kornienko O, Latuske P, Kohler L, Allen K (2016) Visual landmarks sharpen grid cell metric and confer context specificity to neurons of the medial entorhinal cortex. Elife 5:e16937. CrossRef Medline

Schmidt-Hieber C, Häusser M (2013) Cellular mechanisms of spatial navigation in the medial entorhinal cortex. Nat Neurosci 16:325–331. CrossRef Medline

Stensola H, Stensola T, Solstad T, Frøland K, Moser MB, Moser EI (2012) The entorhinal grid map is discretized. Nature 492:72–78. CrossRef Medline

Yoganarasimha D, Rao G, Knierim JJ (2011) Lateral entorhinal neurons are not spatially selective in cue-rich environments. Hippocampus 21:1363–1374. CrossRef Medline

Yoon K, Buice MA, Barry C, Hayman R, Burgess N, Fiete IR (2013) Specific evidence of low-dimensional continuous attractor dynamics in grid cells. Nat Neurosci 16:1077–1084. CrossRef Medline

Yoon K, Lewallen S, Kinkhabwala AA, Tank DW, Fiete IR (2016) Grid cell responses in 1D environments assessed as slices through a 2D lattice. Neuron 89:1086–1099. CrossRef Medline

3

FIELD-TO-FIELD VARIABILITY OF GRID CELLS AND TEMPORAL CODING

3.1 SUMMARY

When rodents are freely moving in a 2d arena the firing fields form a hexagonal pattern spanning the environment. The mean firing rates vary widely from field to field and are redistributed under contextual modifications. We study whether differences in the higher-order spike statistics, such as burst firing, lead to the field-to-field variations or rate remapping.

We show that the number of spikes per burst does not vary significantly between firing fields. Furthermore, we demonstrate that the burst appearance does not influence the variability between firing fields. Moreover, we observe that the absolute number of bursts varies from field to field but the proportion of bursts compared to all events does not change significantly across firing fields but across cells. Further, we study the relation between rate remapping and theta-frequency oscillations. We demonstrate that theta-phase coding is preserved but we do not observe differences between the first and second half of the theta cycle.

3.2   REFERENCES

1 # Burst activity plays no role for the field-to-field

2 # variability and rate remapping of grid cells.

3

4 ## Firing-field variability of grid cells

5

6 Michaela Poth and Andreas V.M. Herz

7 Bernstein Center for Computational Neuroscience Munich and Faculty of Biology, Ludwig-

8 Maximilians-Universität München, Grosshadernerstrasse 2, 82152 Planegg-Martinsried, Germany

9

10 # Acknowledgements

14

15 # Abstract

16 Grid cells in rodent medial entorhinal cortex are thought to play a key role for spatial navigation.

17 When the animal is freely moving in an open arena the firing fields of each grid cell tend to form a

18 highly regular, hexagonal lattice spanning the environment. However, firing rates vary from field to

19 field and change under contextual modifications, whereas the field locations do not shift under such

20 "rate remapping". The observed differences in firing rate could reflect overall activity changes or

21 changes in the detailed spike-train statistics. As these two alternatives imply distinct neural coding

22 schemes, we investigated whether temporal firing patterns vary from field to field and whether they

23 change under rate remapping. Focusing on short time scales, we found that the proportion of bursts

24 compared to all discharge events is similar in all firing fields of a given grid cell and does not

25 change under rate remapping. Mean firing rates with and without bursts are proportional for each

26 cell. However, this ratio varies across cells. Additionally, we looked at how rate remapping relates

27 to entorhinal theta-frequency oscillations. Theta-phase coding was preserved despite firing-rate

28 changes from rate remapping but we did not observe differences between the first and second half

29 of the theta cycle, as had been reported for CA1. Our results indicate that both, the heterogeneity

30 between firing fields and rate remapping, are not due to altered firing patterns on short time scales

31 but reflect location-specific changes at the firing-rate level.

32

Keywords

34 entorhinal cortex, grid cell, firing field, burst activity, rate remapping, variability, spatial navigation

35

Introduction

37 As a rodent moves through an open arena, the firing fields of each grid cell in the animal's medial

38 entorhinal cortex (mEC) form an imaginary hexagonal grid tessellating the explored space (Hafting

39 et al., 2005). Despite the striking spatial regularity of these lattices, firing rates vary from field to

40 field by up to an order of magnitude (Diehl et al., 2017; Dunn et al., 2017; Ismakov et al., 2017).

41 These firing-rate variations are stable across time within a session, between repeated sessions, and

42 even after rescaling the arena. When non-spatial cues are altered, however, the field-specific firing

43 rates change even though the firing fields do not shift (Diehl et al., 2017; Ismakov et al., 2017). This

44 phenomenon, known as "rate remapping", indicates that grid-cell activity represents spatial relations

45 as well as contextual cues.

46 Grid cells encode spatial information not only at the level of firing rates but also on shorter time

47 scales: During the traversal of a firing field, the spikes of a grid cell tend to occur at successively

48 earlier phases of the theta-band-filtered local field potential (Hafting et al., 2008, Jeewajee et al.,

49 2014). This phase-precession signal is present at the single-run level (Reifenstein et al., 2012;

50 Reifenstein et al., 2014), underscoring its potential role for behavior. High-frequency bursts with

51 discharge rates of up to 300 Hz are often observed (Latuske et al., 2015) and might carry additional

52 information.

53 Theoretical studies suggest that sensory stimuli can be encoded on fast time scales by modulating

54 the number of spikes that occur within a burst (Kepecs & Lisman, 2003) and such graded burst

55 coding has been revealed in various neural systems (Krahe and Gabbiani, 2004; Eyherabide et al.,

56 2009; Avila-Akerberg et al., 2010). These observations raise the question whether the field-specific

57 firing-rate differences between the multiple firing fields of a given grid cell might reflect field-

58 specific spike-train statistics, in particular at short time scales.

To address this question, we reanalyzed grid-cell data from rats foraging in a square enclosure whose wall colors could be changed from black to white (Diehl et al., 2017). We asked whether the burst length or the number of bursts differed when the multiple firing fields of a grid cell were compared. We found that the heterogeneity between firing fields as well as the firing-rate redistribution during rate remapping were unrelated to burst firing. The relative frequency of burst events varied from cell to cell, in agreement with previous findings (Latuske et al., 2015, Csórdas et al., 2019).

Moreover, we asked whether the heterogeneity between firing fields in a grid cell varies throughout the theta cycle. Theoretical and experimental work suggests different computational roles during different theta phases. For example, Sanders et al. (2015) proposed that the first half of a theta cycle is used for the computation of the animal's present position while future positions are estimated in the cycle's second half. According to our analysis such a functional distinction is not present in the field-to-field variability or rate remapping of grid cells.

Taken together, our results show that burst activity is neither needed to explain the firing-rate variability between the different firing fields of a grid cell nor does it play a role for rate remapping. Both phenomena are fully captured within the classical firing-rate picture. This suggests that the context-dependent modulation of grid-cell activity does not involve inputs that are precisely tuned in time but rather provide a smooth increase or decrease of grid-cell excitability.

Material and Methods

Data

We reanalyzed grid-cell data from Diehl et al. (2017), who had recorded 38 grid cells from seven adult male Long Evans rats foraging in a squared enclosure (100 x 100 cm). We excluded two cells from our analysis that showed a very large fraction (more than 33%) of interspike intervals below 4ms. During training and recording, rats explored the arena in blocks of four 10-minute sessions, and were given five minutes between sessions to rest in a box away from the foraging enclosure. The walls of the foraging enclosure were either all black (B) or all white (W) and altered according to a WBB'W' or BWW'B' paradigm. The starting color was chosen randomly. Between sessions the enclosure's floor was cleaned with water. Prior to any electrophysiological recordings, all enclosures were made highly familiar over at least six training days. Behavioral procedures while recording mEC units were identical to training procedures. For details, see the original study.

Firing-field identification

Similar to Diehl et al. (2017) we constructed firing-rate maps by first summing the total number of spikes that occurred in a given spatial bin (2x2 cm), then dividing by the total amount of time that

92 the rat spent in that bin, and finally smoothing with a Gaussian filter (width: 2.5 cm). To control for

93 possible influences of stationary periods, rate maps were also constructed from data for which the

94 animal's running speed was above 5 cm/s. Firing-field boundaries were calculated by generating a

95 single reference rate map for the four sessions of one recording block. This map was constructed by

96 averaging the rate maps of the four 10-min sessions. The minimum peak rate required for a field

97 was 2 Hz, the minimum field size was 250 cm^2.

98 We then calculated the local maxima of the reference map. Starting from their locations, field

99 boundaries were defined by constructing contours outwards until a threshold value of 0.3 times the

100 individual peak rates was reached. When two fields fused, the threshold value of the higher local

101 maximum was stepwise increased again until the two fields split. The field boundaries derived from

102 the reference map defined the firing field in all four sessions, and all analyses were done for each

103 field in each session. For each such field, the mean field rate was taken as the number of spikes in

104 that field divided by the respective dwell time.

105 **Rate-vector comparisons**

106 To represent the field-specific mean firing rates, we collected their values into one vector for every

107 session. For grid cells with at least 3 firing fields, rate vectors were then compared across sessions

108 using Spearman's rank correlation. To compare rate vectors to chance, shuffled firing-rate vectors

109 were generated by permuting grid fields such that rate vectors of each grid cell were populated by

110 randomly selected mean firing-field rates.

111 **Statistical analysis**

112 All analyses were performed in Python 2.7 (RRID: SCR_008394). Specific statistical tests used are

113 stated throughout the text and were taken from Python scipy.stats (RRID: SCR_008058).

114 **Poisson process**

115 To compare the measured discharge patterns with model spike trains that result in the same rate

116 maps but lack intrinsic bursts, we constructed surrogate spike trains for each recording session of a

117 given grid cell. To do so, we generated rate-modulated Poisson spike trains by using the original

118 rate maps and animal trajectories. As the total number of model spikes in each field might deviate

119 from the measured spike count, we first doubled the firing rates and then randomly drew as many

120 spikes as the original firing field contained. This approach assures that the simulated and the

121 original firing fields have the same mean firing rate.

122 **Spike-train characteristics**

123 Spike-train autocorrelations and inter-spike interval (ISI) distributions were calculated from binned

124 data. The bin width was 2 ms. For the field-wise comparison of autocorrelations and short ISIs, the

spike times of single runs through each firing field were concatenated with a 10 sec interval between the last spike of a run and the first spike of the next run through the same field. A burst was defined as at least two spikes separated by an ISI of less than 10 ms. To compare ISI distributions on time scales relevant for burst firing, the distributions were first normalized in the window from 0 ms to 20 ms.

Extraction of theta-band oscillations and theta phases from the local field potential

Diehl et al. 2017 recorded not only single-unit activity but also the continuous local field potential (LFP). To extract theta-band oscillations, we filtered the LFP signal with a butterworth bandpass filter (6-11 Hz). The theta phase of a spike was then calculated using the Hilbert transform (taken from Python scipy.signal (RRID:SCR_008058)) of the filtered LFP. We used the convention that 0° denotes the LFP peak. Spike phase histograms were built with 36 bins, each 10° wide, and were normalized by the total number of spikes occurring during the recording.

Results

Modifications in contextual cues cause firing-rate changes in rodent grid cells that differ from firing field to firing field, a phenomenon known as "rate remapping" (Diehl et al., 2017, Ismakov et al., 2017). These changes might reflect changes in the higher-order spike-train statistics or occur independently of fine temporal details in neural activity. To distinguish between these functionally distinct alternatives, we re-analyzed grid-cell data recorded by Diehl et al. (2017). For details, see Material and Methods. These recordings were obtained from the dorsal medial entorhinal cortex (mEC) while rats randomly foraged in a square enclosure (100 x 100 cm) whose walls were black for two sessions (B/B') and white for two sessions (W/W'). The order of the wall colorations was either BWW'B' or WBB'W' and the starting color was chosen randomly. Each block consisted of four 10-minute recording sessions with 5-minute pauses in between, as shown in Figure 1a for a BWW'B' session. The location of grid fields (see also Material and Methods: Firing-field identification) remained constant but the field-specific firing rates changed (Figure 1b). This can readily be seen by calculating the mean firing rate for each firing field and entering these values into a rate vector (see Material and Methods). Comparing these vectors across the four sessions of each cell (Figure 1c) shows that the firing rates of corresponding fields are similar between sessions with matching colors but not across sessions with non-matching colors, as reported by Diehl et al. (2017).

Heterogeneity between firing fields is not the result of altered burst firing

Consistent with previous reports (Diehl et al., 2017, Dunn et al., 2017, Ismakov et al., 2017), we observed that within a given environment grid-cell firing rates varied strongly from field to field. To quantify this finding, we calculated the coefficient of variation (CV) of the mean in-field firing rates from the firing-rate maps of each cell and session. Across these samples, we obtained an average CV of 0.40 (Figure 2a).

If this variability resulted from differences in burst firing, the CV should decrease strongly after bursts have been removed from the analysis. In a next step, we therefore excluded all spikes following another spike with an inter-spike interval (ISI) of less than 10ms ("without burst") so that only isolated spikes and the first spike of each burst remained for the analysis. The CV distributions of the mean in-field firing rates without bursts had an average CV of 0.39 and were indistingishable from those with bursts (two-sample t-test: statistic=0.71, p-value=0.48). Repeating the same analyses with a cut-off of 6ms or 8ms did not change the results (data not shown). Furthermore, for each recording the mean burst length was highly similar across firing fields (average CV: 0.06) (Figure 2b). These data demonstrate that burst firing does not explain the heterogeneity in firing between the firing fields of each grid cell and session.

Rate remapping does not hint at changes in burst firing

Although the firing-field variability within one enclosure does not hint at differences in burst firing, burst firing might change under rate remapping. To tackle this possibility, we performed two analyses to detect similarities or differences in burst behavior. First, we compared the four ISI histograms of a given grid cell and focused on ISI-values relevant for burst firing (ISI<20ms). We observed that ISI histograms were similar across different conditions but differed from cell to cell, as shown by the two example cells in Figure 3a. We quantified this finding by calculating the Kullback–Leibler (KL) divergence between the normalized probability density functions of the ISI distributions for WW (W/W'), BB (B/B'), and BW (B/W, B/W', B'/W and B'/W') and compared the distributions using a Kolmogorov-Smirnov (KS) test. This test showed that the ISI distributions were similar in the white and black boxes (WW vs. BB: KS test: statistic=0.18, p-value=0.62; WW vs. BW: KS test: statistic=0.14, p-value=0.63; BB vs. BW: KS test: statistic=0.15, p-value=0.51). In contrast, the ISI histograms differed from cell to cell. This can be seen by comparing the KL divergence across environments with the distribution across cells (KS test: statistic=0.45, p-value=8.98e-11). We then wondered whether the same holds true for spike-train autocorrelations. In a first step, we calculated the Pearson-Correlation-Coefficient of matching (median correlation coefficient for WW across all neurons: r=0.85; for BB: r=0.85) and non-matching colors (r=0.83). A

191 KS test showed that the three distributions were similar (WW vs. BB: statistic=0.18, pvalue=0.62;
192 WW vs. BW: statistic=0.18, pvalue=0.29; BB vs. BW: statistic=0.15, pvalue=0.50), as depicted in
193 Figure 3b for same two example cells as in Figure 3a. As a control, we created sets of surrogate
194 data. To this end, we combined spike-train autocorrelations from two different cells and calculated
195 the Pearson-Correlation-Coefficient of matching (median correlation coefficient for WW surrogate:
196 r=0.63; for BB surrogate: r=0.69) and non-matching colors (BW surrogate r=0.64). The KS test
197 showed a significant difference of the WW/WW surrogate (statistic = 0.53, p-value: 7.29e-05), BB/
198 BB surrogate (statistic = 0.50, p-value = 2.20e-04), and BW/BW surrogate (statistic = 0.53, p-value
199 = 2.07e-07). We conclude that there are significant cell-to-cell differences in the ISI distributions
200 and spike-train autocorrelations but no contextual changes when all firing fields of a grid cell are
201 considered together.

202 Next, we evaluated whether the redistribution of mean in-field firing rates across grid fields results
203 from differences in bursting behavior. To this end, we counted the absolute and relative number of
204 bursts within each grid field and entered these values into a vector for each grid cell and each 10-
205 min session (Figure 3c). By comparing the vectors across sessions, we confirmed that the absolute
206 number of bursts were similar between sessions with matching box colors (median Spearman's rank
207 correlation for WW: 0.80; for BB: and 0.82) as shown in Figure 3d. For non-matching box colors
208 we observed a weaker correlation (median Spearman's rank correlation: 0.40). Label shuffling led
209 to a median Spearman's rank correlation of 0.00. This demonstrates that the correlations between
210 sessions in matching and non-matching box colors are significant (KS test for WW: statistic=0.54,
211 p-value=1.16e-09; for BB: statistic=0.67, p-value=1.03e-14; for BW: statistic=0.21, p-value=4.14e-
212 06). In contrast, the relative number of bursts shows a low median Spearman's rank correlation for
213 the matching and non-matching cases (median Spearman's rank correlation for WW: 0.37; for BB:
214 0.39; for BW: 0.03) as depicted in Figure 3d. Label shuffling indicates that the correlations are
215 weakly significant (KS test for WW: statistic: 0.25, p-value: 0.02; for BB: statistic: 0.24, p-value:
216 0.02) for matching colors and not significant for non-matching colors (KS test: statistic=0.11,
217 p-value=0.08). The relative number of bursts rather fluctuates around one specific value, which
218 varies from cell to cell. We also did not see effects that depend on the order of box-color changes.
219 This indicates that the redistribution of the firing rates in the color-change paradigm is not the result
220 of altered burst firing.

221

222 **Mean in-field firing rates with and without bursts are proportional for each cell**

223 As changed burst firing is neither required to explain rate remapping nor the firing-rate variability
224 across fields, we expected that in-field firing rates with and without bursts were correlated. Indeed,

225   we observed a linear relation between the firing rate with and without bursts (Figure 4a). For each

226   cell, a linear regression line fits the data well (p-values < 1.35e-05). The slopes vary between 0.62

227   and 0.95 and the intercepts between -0.20 and 0.57 (Figure 4b). Since the distributions are similar

228   for black and white environments (Wilcoxon-rank sum test: slope: statistic=293.0, p-value=0.53,

229   intercept: statistic=236.0, p-value=0.43), we pooled the data for each cell across environments.

230   However, the variability in the slopes did not appear compatible with a simple Poisson process. To

231   quantify this finding, we simulated spike trains generated with inhomogeneous Poisson processes

232   based on the individual firing-rate maps and animal trajectories (Materials and Methods) and

233   repeated the previous analysis. To create model spike trains without "bursts", we removed all spikes

234   following an inter-spike interval of less than 10ms. We again found a linear relation between the

235   mean in-field firing rate with and without "bursts" (Figure 4c). The distribution of the slopes ranged

236   from 0.75 to 0.94 (Figure 4d) and differed from the original data (Wilcoxon-rank sum test: slope:

237   statistic=6.0, p-value=2.79e-07). This was to be expected as for a Poisson process, the relation

238   between the number of "bursts" and the number of all events is similar in each firing field. These

239   findings underscore that grid-cell firing deviates from Poisson spiking but do not hint at a particular

240   role of burst events.

241

Rate remapping is not reflected in the local field potential

243   In line with previous work (Hasselmo et al., 2002; Sanders et al., 2015), Sanders et al. (2018)

244   provided evidence that under hippocampal rate remapping, the two halves of the theta cycle have

245   different functions for place cells in CA1, but not in CA3. For each cell, these authors compared

246   place fields in which rate remapping was observed. On a place-field-by-place-field basis, they

247   defined a "low-rate condition" as the condition for which the cell's firing rate (in that particular

248   field) was lower than in the other condition, named "high-rate condition" (for that field). In the low-

249   rate condition, place cells in CA1 tended to spike during the second half of the theta cycle while the

250   first half was preferred in the high-rate condition. This type of theta-phase dependence was not

251   observed in CA3. The medial entorhinal cortex, populated by grid cells, projects both directly and

252   indirectly to CA1 and CA3. This raises the question whether grid-cell firing under remapping is

253   reminiscent of place-cell firing in CA1 or place-cell firing in CA3 or shows yet another behavior.

254   Before we address this question, let us first ask whether for a given environment, spike phases differ

255   between grid fields with higher rate and fields with lower rate. To this end, we constructed – for

256   each grid cell and recording – a polar histogram of the spikes occurring in the grid field with the

257   highest mean firing rate and of the spikes occurring in the grid field with the lowest mean firing

258   rate. We then calculated the (circular) difference of the circular means of both histograms for each

recording session (Figure 5a). Across cells and sessions, circular statistics gives a mean difference of -7° with a standard deviation of 52° (Figure 5b, left panel). These data suggest that field-to-field differences in the firing rates of a given grid cell are not mirrored in phase differences relative to the LFP.

Still, rate remapping could cause phase shifts. Following Sanders et al. (2018), we compared high-rate and low-rate conditions across differently colored environments (BW). Circular statistics did not reveal significant differences in the theta-phase preferences between the high-rate and the low-rate conditions (mean = 1°, std = 55°), as shown in the middle panel of Figure 5b. As a control, we also compared high-rate vs. low-rate conditions from the first and second recording with the same coloring (WW or BB). Here, we obtained a mean of -4° (std = 43°), see the right panel of Figure 5b. We conclude that mEC grid cells do not show the firing-rate-dependent phase-preferences of CA1 place cells but rather the characteristics of CA3 cells. This suggests that the behavior exhibited by CA1 place cells is not caused by mEC grid-cell inputs.

Discussion

Grid cells encode spatial information not only in their firing-rate based activity fields but also at a finer temporal scale via theta-range phase precession (Hafting et al., 2008). In addition, grid cells represent contextual information through field-to-field variations in their firing rates (Diehl et al., 2017; Ismakov et al., 2017). Whether these variations are due to differences in the higher-order spike statistics, such as burst firing, or simply result from different activity levels has not been addressed in the literature. To tackle this question, which is key for a comprehensive understanding of the grid-cell code, we investigated the fine-scale temporal behavior of grid cells field-by-field and studied its potential impact on the firing-rate variability.

It has been suggested that burst duration might encode information (Kepecs and Lisman., 2003), and indeed, burst duration coding is present in other neural systems (Eyherabide et al., 2009, Avila-Akerberg et al., 2010). However, in the grid-cell data analyzed in the present study, the number of spikes per burst does not vary significantly between firing fields. Furthermore, we found that the appearance of bursts does not influence the heterogeneity between firing fields. We also did not find differences in the ISI distributions (ISI < 20 ms) and the autocorrelations of each grid cell within the same or across differently colored enclosures. Furthermore, although the absolute number of bursts varied from field to field, the ratio between bursts and all events was constant between fields and recording sessions. This indicates that individual grid cells have a specific bursting behavior and the redistribution of the firing rates across their grid fields is not the result of modified burst firing. This

292 finding is supported by the observation that in all firing fields of a given grid cell the mean firing

293 rates with and without bursts are proportional. Different cells, however, differ in their burst

294 behavior. This is consistent with the existence of bursty and non-bursty grid cells (Latuske et al.,

295 2015, Csórdas et al., 2019). It remains an open question whether the burstiness of a grid cell differs

296 in novel versus familiar environments.

297 Our analysis shows that neither the heterogeneity of the firing fields of a given grid cell nor the

298 redistribution of its firing rates under contextual changes is the result of altered burst firing. These

299 results are in line with findings in CA1 and CA3, which demonstrate that hippocampal rate

300 remapping is not the result of modulations in burst firing (Sanders et al., 2018). We have also shown

301 that neither the heterogeneity of the firing rates nor rate remapping leads to changes in the preferred

302 spike phases. This is in line with results shown for rate remapping of place cells in CA3 but not

303 with the results of place cells in CA1 (Sanders et al., 2018). The grid cells analyzed by Diehl et al.

304 (2017) reside in superficial mEC layers which directly project to CA1 and CA3. In contrast to phase

305 precession phenomena (Schlesiger et al., 2015), the preferred spike phases during rate remapping in

306 CA1 can thus not be inherited form grid cells. More generally, our findings suggest that the field-to-

307 field variability of grid-cell firing and its context-dependent modulation are not caused by precisely

308 timed inputs but rather by a gradual increase or decrease of grid-cell excitability.

References

Ávila-Åkerberg, O., Krahe, R., & Chacron, M. J. (2010). Neural heterogeneities and stimulus properties affect burst coding in vivo. *Neuroscience 168,* 300-313. http://dx.doi.org/10.1016/j.neuroscience.2010.03.012

Csordás, D. E., Fischer, C., Nagele, J., Stemmler, M., & Herz, A. V. M. (2019). Spike afterpotentials shape the in-vivo burst activity of principal cells in medial entorhinal cortex. *BioRxiv,* 10.1101/841346. http://dx.doi.org/10.1101/841346

Diehl, G.W., Hon, O.J., Leutgeb, S., & Leutgeb, J. K. (2017). Grid and nongrid cells in medial entorhinal cortex represent spatial location and environmental features with complementary coding schemes. *Neuron, 94,* 83-92. http://dx.doi.org/10.1016/j.neuron.2017.03.004

Dunn, B., Wennberg, D., Huang, Z., & Roudi, Y. (2017). Grid cells show field-to-field variability and this explains the aperiodic response of inhibitory interneurons. *arXiv,* 1701.04893v1. http://dx.doi.org/10.1101/101899

Eyherabide, H. G., Rokem, A., Herz, A. V. M., & Samengo, I. (2009). Bursts generate a non-reducible spike-pattern code. *Frontiers in Neuroscience, 3,* 8-14. http://dx.doi.org/10.3389/neuro.01.002.2009

Hafting, T., Fyhn, M., Molden, S., Moser, M.-B., & Moser, E.I. (2005). Microstructure of a spatial map in the entorhinal cortex. *Nature, 436,* 801–806. http://dx.doi.org/10.1038/nature03721

Hafting, T., Fyhn, M., Bonnevie, T., Moser, M. B., & Moser, E. I. (2008). Hippocampus independent phase precession in entorhinal grid cells. *Nature, 453,* 1248-1252. http://dx.doi.org/10.1038/nature06957

Hasselmo, M.E., Bodelón, C., & Wyble, B.P. (2002). A proposed function for hippocampal theta rhythm: separate phases of encoding and retrieval enhance reversal of prior learning. *Neural Computation, 14,* 793-817. http://dx.doi.org/10.1162/089976602317318965

Ismakov, R., Barak, O., Jeffery, K., & Derdikman, D. (2017). Grid cells encode local positional information. *Current Biology, 27,* 2337-2343. http://dx.doi.org/10.1016/j.cub.2017.06.034

Jeewajee, A., Barry, C., Douchamps, V., Manson, D., Lever, C., & Burgess, N. (2014). Theta phase precession of grid and place cell firing in open environments. *Phil. Trans. R. Soc. B 369,* 20120532. http://dx.doi.org/10.1098/rstb.2012.0532

Kepecs, A., & Lisman, J. (2003). Information encoding and computation with spikes and bursts. *Network: Computation in Neural Systems, 14,* 103-118. http://dx.doi.org/10.1080/net.14.1.103.118

Krahe, R., & Gabbiani, F. (2004). Burst firing in sensory systems. *Nature Reviews Neuroscience, 5,* 13-22. http://dx.doi.org/10.1038/nrn1296

Latuske, P., Toader, O., & Allen, K. (2015). Interspike intervals reveal functionally distinct cell populations in the medial entorhinal cortex. *Journal of Neuroscience, 35,* 10963–10976. http://dx.doi.org/10.1523/JNEUROSCI.0276-15.2015

Reifenstein, E.T., Kempter, R., Schreiber, S., Stemmler, M. B., & Herz, A. V. M. (2012). Grid cells in rat entorhinal cortex encode physical space with independent firing fields and phase precession at the single-trial level. *Proc. Natl. Acad. Sci. USA, 109,* 6301–6306. http://dx.doi.org/10.1073/pnas.1109599109

Reifenstein, E.T, Stemmler, M. B. , Herz, A. V. M., Kempter, R., & Schreiber, S. (2014) Movement dependence and layer specificity of entorhinal phase precession in two-dimensional environments. *PLoS one, 9,* e100638. http://dx.doi.org/10.1371/journal.pone.0100638

Sanders, H, Rennó-Costa, C., Idiart, M., & Lisman, J. (2015). Grid cells and place cells: an integrated view of their navigational and memory function. *Trends in Neurosciences, 38,* 763-775. http://dx.doi.org/10.1016/j.tins.2015.10.004

Sanders, H., Daoyun, J., Sasaki, T., Leutgeb, J. K., Wilson, M. A., & Lisman, J. E. (2018). Temporal coding and rate remapping: Representation of nonspatial information in the hippocampus. *Hippocampus, 2018,* 1-17. http://dx.doi.org/0.1002/hipo.23020

Schlesiger, M. I., Cannova, C. C., Boublil, B. L., Hales, J. B., Mankin, E. A., Brandon, M. P., Leutgeb, J. K., Leibold, C., & Leutgeb, S. (2015). The medial entorhinal cortex is necessary for temporal organization of hippocampal neuronal activity. *Nature Neuroscience, 18,* 1123. http://dx.doi.org/10.1038/nn.4056
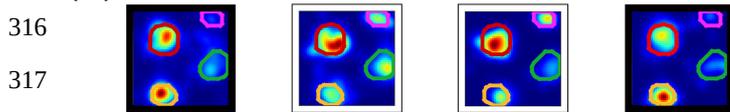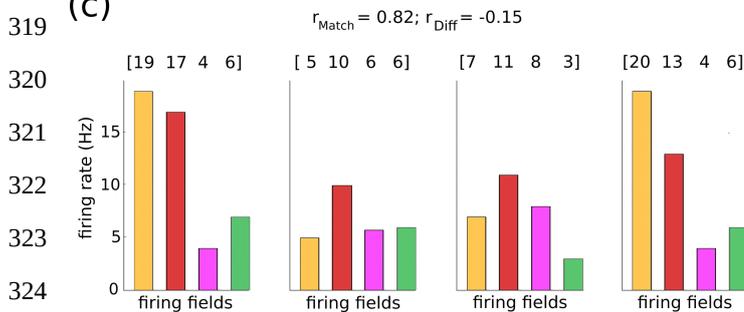
Figures

Figure 1: Remapping of grid-cell firing rates.

(a) Schematic drawing of the experimental paradigm. With interleaved resting periods, the animal explored a square box whose wall colors were altered between black and white according to a BWW'B' or WBB'W' sequence. (b) Firing-rate maps of an example grid cell that was recorded across all four conditions. The individual firing fields are encircled by a colored line. Shape and position of each firing field is almost identical in all four conditions. (c) Mean firing rates, in matching colors, for the four fields shown in (b). The Rate Vectors (RVs) above the color bars represent the mean firing rates within each grid field. The average Spearman correlation of the RVs is high between matching conditions but low across different conditions.
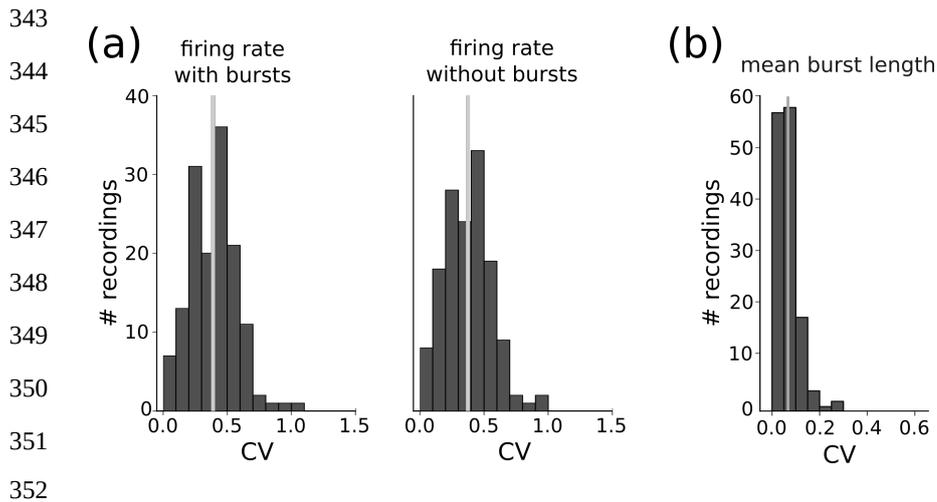
Figure 2: Heterogeneity of firing fields is not caused by burst activity.

(a) Population results for the firing-rate variability. For each grid cell and recordings session, firing fields were identified and mean discharge rates were computed field-by-field. Their variability was measured in terms of the coefficient of variation (CV) and averaged across sessions and cells. The left panel is based on the original spike data. For the second panel burst-like discharges were discarded by removing all spikes with a preceding inter-spike interval (ISI) of less than 10 ms. (b) Population results for the burst-length variability, calculated as the CV of the number of spikes within a burst.

Figure 3: Rate remapping does not hint at changes in burst firing.
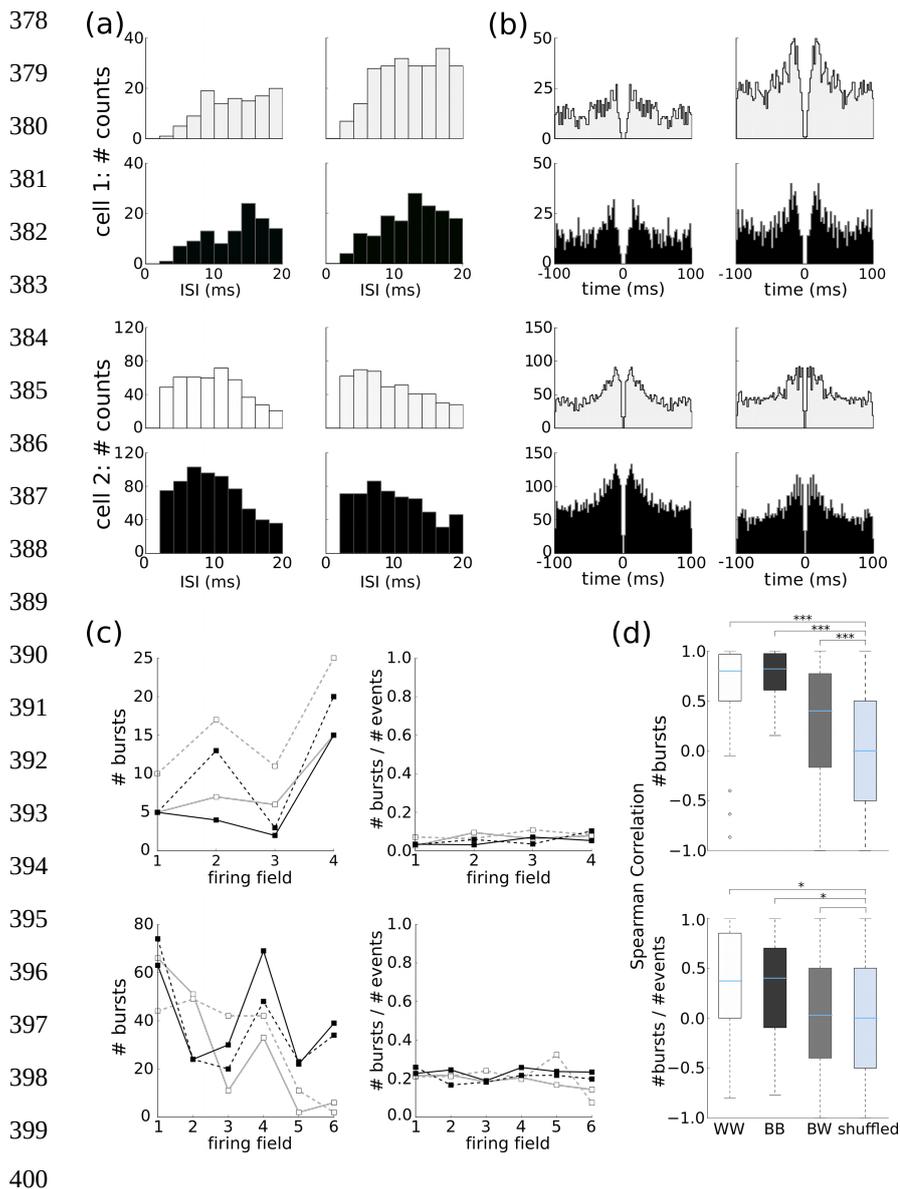
(a) ISI histograms and (b) autocorrelations of two example cells. The white and black colors of the filled areas mark the colors of the respective enclosure walls. (c) Number of bursts per firing field (left) and relative number of bursts (right). Black/white enclosures are indicated by lack/grey lines, respectively. Line style denotes the first (solid) and second (dashed) session in that enclosure. (d) Population results of the absolute and relative burst numbers across all cells, as quantified by Spearman Correlations for the specific wall combinations WW, BB and BW, as well as for shuffled labels. Blue lines indicate the population median.
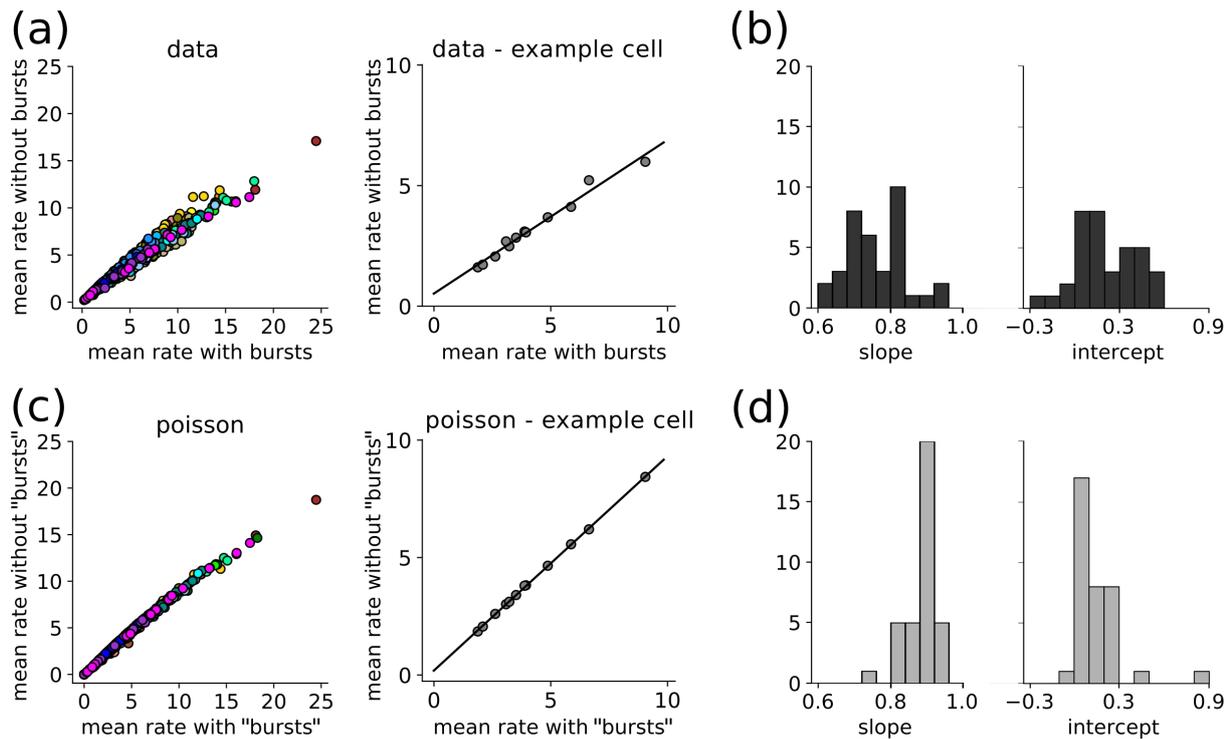
Figure 4: Mean firing rates with and without bursts are proportional.
(a) Each dot represents the mean firing rate in a firing field calculated with all spikes ("with bursts") on the x-axis and after spikes with a previous ISI < 10 ms were removed ("without bursts") on the y-axis. Left panel: Population results. Firing fields of a specific cell have the same color. Right panel: One example cell, together with the linear regression line. (b) Population results from measured grid cells: Distribution of the linear regression slopes (left column) and distribution of the linear regression intercepts (right column). (c) Model firing rate maps were simulated with inhomogeneous Poisson processes that were based on the original firing rate maps and movement patterns. The firing field sizes and positions as well as the number of spikes per firing field are exactly the same than in the original data. Left panel: Population results. As in (a), the firing fields of a specific cell have the same color. Right panel: One example cell, together with the linear regression line. (d) Population results as in (b) but now from the Poisson model.
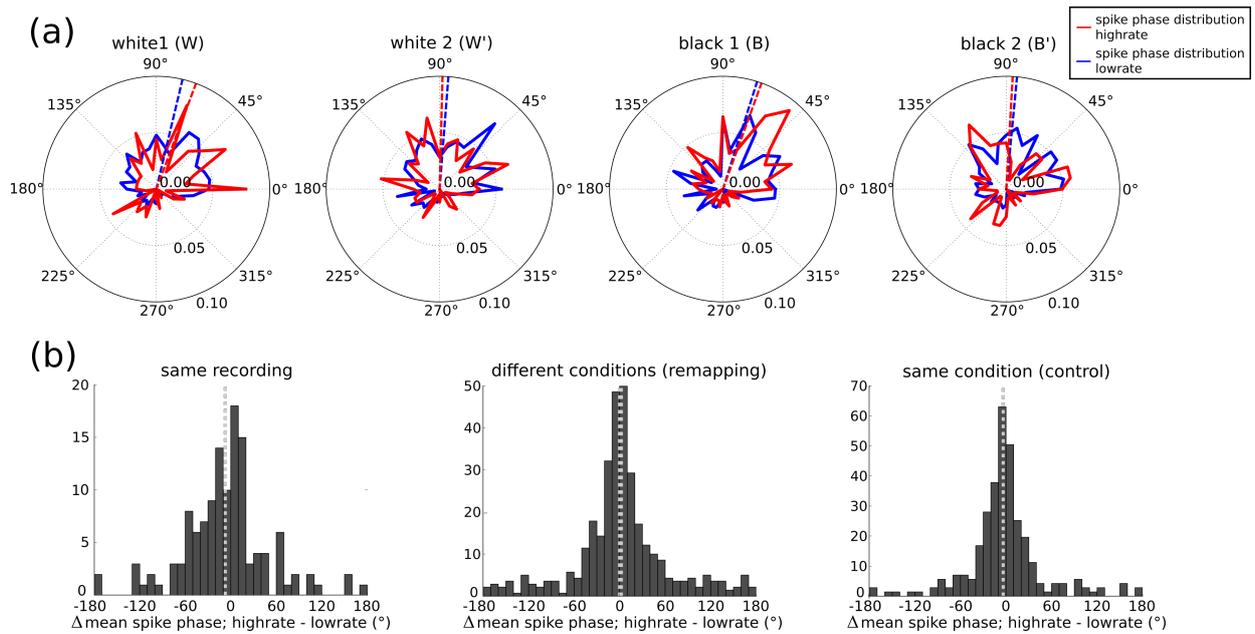
Figure 5: Spike phases do not differ between high and low firing rates.

(a) For one example cell, distributions of spike phases relative to the theta-band oscillation in the local field potential (LFP) are shown for the four environments (W, W', B, B'). Red (blue) curves represent the spike phases in the firing field with the highest (lowest) mean firing rate. Dashed lines mark the circular means of the two distributions. (b) The differences between the circular mean of the spike phase distribution in the high rate condition and the low rate condition are shown. For the left panel the high/low rate condition is defined as in Figure 5A, i.e., as the firing field with the highest/lowest mean firing rate within each recording. All four environments are treated independently and the differences between the two circular means (high rate minus low rate) are collected across cells and environments. In the middle panel we compared spike phases from the same firing fields under rate remapping, as Sanders et al. (2018) did for hippocampal place cells. Accordingly, high/low-rate condition is defined as the condition with the higher/lower mean firing rate for that particular firing field. All scenarios (W/B, W/B', W'/B, and W'/B') are considered across all cells. In the right panel we compare, as a control, the recordings from the two white/black environments of each cells. The two possible combinations (W/W' and B/B') are pooled across all cells. In the third panel we considered the recording from the white and the black environments of each cell. As the position of each firing fields is the same in all four recording sessions, we compared the spike phase distributions for each firing field in W/B, W/B', W'/B, and W'/B'. We defined the high/low-rate condition as the firing field with the higher/lower mean firing rate. For each firing field the circular means of the phase distributions were calculated. The distribution of the differences of the circular means are shown across cells. In all three panels the light grey dotted line denotes the circular mean of the respective distribution.

4

DISCUSSION, CONCLUSION AND OUTLOOK

In this thesis, we study the heterogeneity of firing rates in grid cells. The field-to-field variability of grid cells' activity has been observed for movements along linear tracks as well as in 2d environments. Here, we investigate the phenomenon in both, 1d and 2d environments. The scope, however, is different. In chapter 2, we explain the field-to-field variability in 1d environments by a pure rate coding approach. In chapter 3, by contrast, we are interested in the temporal code underlying the field-to-field variability in 2d environments.

Let us start with grid cell activity on a linear track, a quasi 1d environment. When an animal runs along such a track the firing rates vary widely from field to field and the firing patterns of left to right and right to left runs seem to differ [19]. As shown in chapter 2, this can be explained by slices through a highly regular 2d hexagonal firing pattern if a translational shift is allowed when the animal turns around and runs in the opposite direction [95]. In this part of the thesis, we assume a pure rate coding mechanism and ignore information possibly encoded in the spike-trains temporal structure. In 1926, Adrian and Zotterman have already shown the existence of rate coding in the motor cortex [2]. Hubel and Wiesel demonstrated in 1968 that the firing rate of neurons in the primary visual cortex encodes information about the orientation of edges or bars of light in their receptive field [52]. In place cells the firing rate also seems to be important for coding because they are active at a certain location

in the environment and silent elsewhere. A good example for rate coding in grid cells and place cells is rate remapping as the position of each firing field remains stable while the firing rate changes (see chapter 3). In chapter 2 we demonstrate that the field-to-field variability on a linear track can be explained by a simple rate model and that this is not only true for one running direction.

However, we cannot exclude that the "real" reason of this variability is another. In the literature, numerous variables are discussed as sources of neural variability [101]. Potential ones are the past experience of the animal, i.e., the history of the experiment [45, 101, 116] or the animal's attention. When the animal pays more attention to the task, a reduction of the neural variability has been reported for example in the areas V1 [51] and V4 [24, 77, 78]. For the data analyzed in chapter 2, this would mean that the animal pays much more attention in one firing field than in another one while it is running with an almost constant (high) speed along the track. Similarly, one can argue against fieldwise differences because of the experiment's history. According to this, it is very unlikely that the animal's attention or the experiment's history is the source of the variability in chapter 2. They might explain differences in the firing from session to session or from run to run but not from field to field.

New experiments could validate our hypotheses that the grid-cell activity along a linear track comes from slices through the 2d hexagonal grid pattern if translational shifts of the pattern are allowed at the movement turning points. Grid cells or conjunctive grid-by-head-direction cells could be recorded in a familiar, large 2d environment as well as on a familiar linear track. Thereby, this track should be positioned without boundaries and with

various orientations in the 2d arena. It is important that the track is long enough to obtain at least four firing fields per running direction. Moreover, several cells of the same module need to be recorded simultaneously to make a statistically significant statement about a common shift of the underlying pattern at the movement turning point. Grid-parameters can be derived from the 2d experiment and compared with the parameters derived from the linear track data according to the procedure suggested in chapter 2. For conjunctive cells, a clearly modulated firing activity is expected when one running direction fits the preferred head direction of the cell, while the cell is inactive for runs in the opposite direction. Moreover, they are silent for both running directions if the linear track is placed in another direction.

In 2017, three studies reported a heterogeneity of the grid cell's firing fields in 2d environments [30, 32, 54]. Furthermore, a redistribution of the firing rates has been shown if the color of the enclosure is changed from black to white or vice versa [30].

As already described above, rate coding is used in various parts of the brain. Therefore, the spike activity of a cell is usually averaged over the course of minutes. Several studies have shown that information is encoded at the level of milliseconds [122]. As there are a number of organisms which can distinguish diverse stimuli within this time frame, sound localization is an example that rate coding might be to slow [120]. Many studies, however, have focused on firing rates and not on the underlying spiking pattern. In chapter 3, we shift our attention to the temporal structure underlying the field-to-field variability or rate remapping.

That both, rate and temporal coding, are important has been observed among others in the mammalian gustatory system [50]. The rate provides the basic taste information such as sweet

while the temporal code might determine its identity such as glucose or fructose [22]. One considerable temporal code is transmitting information via burst firing. Various studies have shown that interspike intervals of subsequent spikes can convey more information about a stimulus than the rate code [23, 46, 98]. Further, it has been reported that information about stimuli can be encoded by the number of spikes per burst whereby this cannot be interpreted by a rate code [38]. Thus, a temporal and a rate code can occur independently of each other. However, if single spikes would be replaced by bursts, one may observe an increase of the firing rate [132]. Moreover, individual neurons can change from bursting to tonic spiking and vice versa [26, 53]. This could lead to the assumption that the field-to-field variability of grid cells recorded in 2d can be explained by field-wise differences in the bursting behaviour. Our analysis in chapter 3 does not support this hypothesis. What's more, we show that the bursting behaviour of a neuron does not change in the case of rate remapping [94]. These results are in line with the findings in CA1 and CA3 place cells [102]. Like in the mammalian gustatory system, the temporal and the rate code of place and grid cells seem to convey different information while rate remapping occurs. In the data analyzed in chapter 3, the firing rate appears to encode the differences of the wall color. The temporal burst ratio, by contrast, stays constant.

However, it is not clear whether grid cells use a burst code as many other cells do. To test this, an analysis similar to the one in chapter 3 could be performed on recordings in different familiar or novel environments. That way, one can investigate whether the bursting behavior changes and, thus, can be applied to encode or transfer information.

BIBLIOGRAPHY

[1]   L. F. Abbott and K. I. Blum. "Functional significance of long-term potentiation for sequence learning and prediction." In: *Cerebral Cortex* (1996). ISSN: 10473211. DOI: 10.1093/cercor/6.3.406.

[2]   E. D. Adrian and Y. Zotterman. "The impulses produced by sensory nerve endings: Part 3. Impulses set up by Touch and Pressure." In: *The Journal of Physiology* (1926). ISSN: 14697793. DOI: 10.1113/jphysiol.1926.sp002308.

[3]   J. A. Ainge, M. Tamosiunaite, F. Wörgötter, and P. A. Dudchenko. "Hippocampal place cells encode intended destination, and not a discriminative stimulus, in a conditional T-maze task." In: *Hippocampus* (2012). ISSN: 10509631. DOI: 10.1002/hipo.20919.

[4]   K. Allen, J. N. P. Rawlins, D. M. Bannerman, and J. Csicsvari. "Hippocampal place cells can encode multiple trial-dependent features through rate remapping." In: *Journal of Neuroscience* (2012). ISSN: 02706474. DOI: 10.1523/JNEUROSCI.6175-11.2012.

[5]   C. B. Alme, C. Miao, K. Jezek, A. Treves, E. I. Moser, and M. B. Moser. "Place cells in the hippocampus: Eleven maps for eleven rooms." In: *Proceedings of the National Academy of Sciences of the United States of America* (2014). ISSN: 10916490. DOI: 10.1073/pnas.1421056111.

[6]   A. Alonso and R. Klink. "Differential electroresponsiveness of stellate and pyramidal-like cells of medial entorhi-

nal cortex layer II." In: *Journal of Neurophysiology* (1993).
ISSN: 00223077. DOI: 10.1152/jn.1993.70.1.128.

[7]   M. I. Anderson and K. J. Jeffery. "Heterogeneous modulation of place cell firing by changes in context." In: *Journal of Neuroscience* (2003). ISSN: 02706474. DOI: 10.1523/jneurosci.23-26-08827.2003.

[8]   D. E. A. T. Arnolds, F. H. Lopes Da Silva, J. W. Aitink, A. Kamp, and P. Boeijinga. "The spectral properties of hippocampal EEG related to behaviour in man." In: *Electroencephalography and Clinical Neurophysiology* (1980). ISSN: 00134694. DOI: 10.1016/0013-4694(80)90160-1.

[9]   D. Aronov, R. Nevers, and D. W. Tank. "Mapping of a non-spatial dimension by the hippocampal-entorhinal circuit." In: *Nature* (2017). ISSN: 14764687. DOI: 10.1038/nature21692.

[10]   O. Avila-Akerberg, R. Krahe, and M. J. Chacron. "Neural heterogeneities and stimulus properties affect burst coding in vivo." In: *Neuroscience* (2010). ISSN: 03064522. DOI: 10.1016/j.neuroscience.2010.03.012.

[11]   J. S. Bant, K. Hardcastle, S. A. Ocko, and L. M. Giocomo. "Topography in the Bursting Dynamics of Entorhinal Neurons." In: *Cell Reports* (2020). ISSN: 22111247. DOI: 10.1016/j.celrep.2020.01.057.

[12]   C. Barry, L. L. Ginzberg, J. O'Keefe, and N. Burgess. "Grid cell firing patterns signal environmental novelty by expansion." In: *Proceedings of the National Academy of Sciences of the United States of America* (2012). ISSN: 00278424. DOI: 10.1073/pnas.1209918109.

[13] C. Barry, R. Hayman, N. Burgess, and K. J. Jeffery. "Experience-dependent rescaling of entorhinal grids." In: *Nature Neuroscience* (2007). ISSN: 10976256. DOI: 10.1038/nn1905.

[14] V. Bekhterev. "Demonstration eines gehirns mit zerstörung der vorderen und inneren theile der hirnrinde beider schläfenlappen." In: *Neurologische Zeitenblatte* 19 (1900), pp. 990–991.

[15] O. Belkind. "Leibniz and Newton on Space." In: *Foundations of Science* (2013). ISSN: 12331821. DOI: 10.1007/s10699-011-9280-5.

[16] S. Bisch and R. Wehner. "Visual navigation in ants evidence for site-based vectors." In: *Proc Neurobiol Conf Göttingen* 26 (1998), p. 417.

[17] B. H. Bland. "The physiology and pharmacology of hippocampal formation theta rhythms." In: *Progress in Neurobiology* (1986). ISSN: 03010082. DOI: 10.1016/0301-0082(86)90019-5.

[18] K. Brun, T. Solstad, V. H. Brun, T. Hafting, S. Leutgeb, M. P. Witter, E. I. Moser, and M. B. Moser. "Finite scale of spatial representation in the hippocampus." In: *Science* (2008). ISSN: 00368075. DOI: 10.1126/science.1157086.

[19] V. H. Brun, T. Solstad, K. Brun Kjelstrup, M.e Fyhn, M. P. Witter, E. I. Moser, and M. B. Moser. "Progressive increase in grid scale from dorsal to ventral medial entorhinal cortex." In: *Hippocampus* (2008). ISSN: 10509631. DOI: 10.1002/hipo.20504.

[20] N. Burgess, E. A. Maguire, and J. O'Keefe. "The human hippocampus and spatial and episodic memory." In: *Neu-*

ron (2002). ISSN: 08966273. DOI: `10.1016/S0896-6273(02)00830-9`.

[21] G. Buzsáki. "Theta oscillations in the hippocampus." In: *Neuron* (2002). ISSN: 08966273. DOI: `10.1016/S0896-6273(02)00586-X`.

[22] A. Carleton, R. Accolla, and S. A. Simon. "Coding in the mammalian gustatory system." In: *Trends in Neurosciences* (2010). ISSN: 01662236. DOI: `10.1016/j.tins.2010.04.002`.

[23] S. M. Chase and E. D. Young. "First-spike latency information in single neurons increases when referenced to population onset." In: *Proceedings of the National Academy of Sciences of the United States of America* (2007). ISSN: 00278424. DOI: `10.1073/pnas.0610368104`.

[24] M. R. Cohen and J. H. R. Maunsell. "Attention improves performance primarily by reducing interneuronal correlations." In: *Nature Neuroscience* (2009). ISSN: 10976256. DOI: `10.1038/nn.2439`.

[25] M. Collett, T. S. Collett, S. Bisch, and R. Wehner. "Local and global vectors in desert ant navigation." In: *Nature* (1998). ISSN: 00280836. DOI: `10.1038/28378`.

[26] D. C. Cooper. "The significance of action potential bursting in the brain reward circuit." In: *Neurochemistry International* (2002). ISSN: 01970186. DOI: `10.1016/S0197-0186(02)00068-2`.

[27] J. Csicsvari, H. Hirase, A. Czurko, and G. Buzsáki. "Reliability and state dependence of pyramidal cell-interneuron synapses in the hippocampus: An ensemble approach in

the behaving rat." In: *Neuron* (1998). ISSN: 08966273. DOI: 10.1016/S0896-6273(00)80525-5.

[28] L. Davachi and I. G. Dobbins. "Declarative memory." In: *Current Directions in Psychological Science* (2008). ISSN: 09637214. DOI: 10.1111/j.1467-8721.2008.00559.x.

[29] D. Derdikman, J. R. Whitlock, A. Tsao, M. Fyhn, T. Hafting, M. B. Moser, and E. I. Moser. "Fragmentation of grid cell maps in a multicompartment environment." In: *Nature Neuroscience* (2009). ISSN: 10976256. DOI: 10.1038/nn.2396.

[30] G. W. Diehl, O. J. Hon, S. Leutgeb, and J. K. Leutgeb. "Grid and Nongrid Cells in Medial Entorhinal Cortex Represent Spatial Location and Environmental Features with Complementary Coding Schemes." In: *Neuron* (2017). ISSN: 10974199. DOI: 10.1016/j.neuron.2017.03.004.

[31] C. Domnisoru, A. A. Kinkhabwala, and D. W. Tank. "Membrane potential dynamics of grid cells." In: *Nature* (2013). ISSN: 14764687. DOI: 10.1038/nature11973.

[32] B. Dunn, D. Wennberg, Z. Huang, and Y. Roudi. "Grid cells show field-to-field variability and this explains the aperiodic response of inhibitory interneurons." In: *arXiv preprint arXiv:1701.04893* (2017).

[33] H. Eichenbaum, M. Kuperstein, A. Fagan, and J. Nagode. "Cue-sampling and goal-approach correlates of hippocampal unit activity in rats performing an odor-discrimination task." In: *Journal of Neuroscience* (1987). ISSN: 02706474. DOI: 10.1523/jneurosci.07-03-00716.1987.

[34] A. D. Ekstrom and C. Ranganath. "Space, time, and episodic memory: The hippocampus is all over the cognitive map." In: *Hippocampus* (2017). ISSN: 10981063. DOI: 10.1002/hipo.22750.

[35] J. Epsztein, M. Brecht, and A. K. Lee. "Intracellular Determinants of Hippocampal CA1 Place and Silent Cell Activity in a Novel Environment." In: *Neuron* (2011). ISSN: 10974199. DOI: 10.1016/j.neuron.2011.03.006.

[36] A. S. Etienne. "The Control of Short-Distance Homing in the Golden Hamster." In: *Cognitive Processes and Spatial Orientation in Animal and Man* (1987). DOI: 10.1007/978-94-009-3531-0_19.

[37] A. S. Etienne and K. J. Jeffery. "Path integration in mammals." In: *Hippocampus* (2004). ISSN: 10509631. DOI: 10.1002/hipo.10173.

[38] H. G. Eyherabide, A. Rokem, A. V. M. Herz, and I. Samengo. "Bursts generate a non-reducible spike-pattern code." In: *Frontiers in Neuroscience* (2009). ISSN: 16624548. DOI: 10.3389/neuro.01.002.2009.

[39] J. Ferbinteanu, P. Shirvalkar, and M. L. Shapiro. "Memory modulates journey-dependent coding in the rat hippocampus." In: *Journal of Neuroscience* (2011). ISSN: 02706474. DOI: 10.1523/JNEUROSCI.1241-11.2011.

[40] S. Finger. *Origins of neuroscience: a history of explorations into brain function*. Oxford University Press, USA, 2001.

[41] M. Fyhn, T. Hafting, A. Treves, M. B. Moser, and E. I. Moser. "Hippocampal remapping and grid realignment in entorhinal cortex." In: *Nature* (2007). ISSN: 14764687. DOI: 10.1038/nature05601.

[42] M. Fyhn, T. Hafting, M. P. Witter, E. I. Moser, and M. B. Moser. "Grid cells in mice." In: *Hippocampus* (2008). ISSN: 10509631. DOI: 10.1002/hipo.20472.

[43] M. Fyhn, S. Molden, M. P. Witter, E. I. Moser, and M. B. Moser. "Spatial representation in the entorhinal cortex." In: *Science* (2004). ISSN: 00368075. DOI: 10.1126/science.1099901.

[44] L. M. Giocomo, T. Stensola, T. Bonnevie, T. Van Cauter, M. B. Moser, and E. I. Moser. "Topography of head direction cells in medial entorhinal cortex." In: *Current Biology* (2014). ISSN: 09609822. DOI: 10.1016/j.cub.2013.12.002.

[45] J. I. Gold, C. T. Law, P. Connolly, and S. Bennur. "The relative influences of priors and sensory evidence on an oculomotor decision variable during perceptual learning." In: *Journal of Neurophysiology* (2008). ISSN: 00223077. DOI: 10.1152/jn.90629.2008.

[46] T. Gollisch and M. Meister. "Rapid neural coding in the retina with relative spike latencies." In: *Science* (2008). ISSN: 00368075. DOI: 10.1126/science.1149639.

[47] K. Gupta, N. J. Beer, L. A. Keller, and M. E. Hasselmo. "Medial entorhinal grid cells and head direction cells rotate with a T-maze more often during less recently experienced rotations." In: *Cerebral Cortex* (2014). ISSN: 14602199. DOI: 10.1093/cercor/bht020.

[48] T. Hafting, M. Fyhn, T. Bonnevie, M. B. Moser, and E. I. Moser. "Hippocampus-independent phase precession in entorhinal grid cells." In: *Nature* (2008). ISSN: 14764687. DOI: 10.1038/nature06957.

[49]   T. Hafting, M. Fyhn, S. Molden, M. B. Moser, and E. I. Moser. "Microstructure of a spatial map in the entorhinal cortex." In: *Nature* (2005). ISSN: 00280836. DOI: 10.1038/nature03721.

[50]   R. M. Hallock and P. M. Di Lorenzo. "Neuroscience and Biobehavioral Reviews." In: (2006). ISSN: 01497634. DOI: 10.1016/j.neubiorev.2006.07.005.

[51]   J. L. Herrero, M. J. Roberts, L. S. Delicato, M. A. Gieselmann, P. Dayan, and A. Thiele. "Acetylcholine contributes through muscarinic receptors to attentional modulation in V1." In: *Nature* (2008). ISSN: 00280836. DOI: 10.1038/nature07141.

[52]   D. H. Hubel and T. N. Wiesel. "Receptive fields and functional architecture of monkey striate cortex." In: *The Journal of Physiology* (1968). ISSN: 14697793. DOI: 10.1113/jphysiol.1968.sp008455.

[53]   B. I. Hyland, J. N. J. Reynolds, J. Hay, C. G. Perk, and R. Miller. "Firing modes of midbrain dopamine cells in the freely moving rat." In: *Neuroscience* (2002). ISSN: 03064522. DOI: 10.1016/S0306-4522(02)00267-1.

[54]   R. Ismakov, O. Barak, K. Jeffery, and D. Derdikman. "Grid Cells Encode Local Positional Information." In: *Current Biology* (2017). ISSN: 09609822. DOI: 10.1016/j.cub.2017.06.034.

[55]   A. Jeewajee, C. Barry, V. Douchamps, D. Manson, C. Lever, and N. Burgess. "Theta phase precession of grid and place cell firing in open environments." In: *Philosophical Transactions of the Royal Society B: Biological Sciences* (2014). ISSN: 14712970. DOI: 10.1098/rstb.2012.0532.

[56] A. Kamondi, L. Acsády, X. J. Wang, and G. Buzsáki. "Theta oscillations in somata and dendrites of hippocampal pyramidal cells in vivo: Activity-dependent phase-precession of action potentials." In: *Hippocampus* (1998). ISSN: 10509631. DOI: 10.1002/(SICI)1098-1063(1998)8:3<244::AID-HIPO7>3.0.CO;2-J.

[57] I. Kant. *Kritik der reinen Vernunft*. 2011. DOI: 10.1515/9783111406855.

[58] W. T. Keeton. "The Orientational and Navigational Basis of Homing in Birds." In: *Advances in the Study of Behavior* (1974). ISSN: 00653454. DOI: 10.1016/S0065-3454(08)60020-0.

[59] A. Kepecs and J. Lisman. "Information encoding and computation with spikes and bursts." In: *Network: Computation in Neural Systems* (2003). ISSN: 0954898X. DOI: 10.1088/0954-898X/14/1/306.

[60] A. Kepecs, X. J. Wang, and J. Lisman. "Bursting neurons signal input slope." In: *Journal of Neuroscience* (2002). ISSN: 02706474. DOI: 10.1523/jneurosci.22-20-09053.2002.

[61] R. Krahe and F. Gabbiani. "Burst firing in sensory systems." In: *Nature Reviews Neuroscience* (2004). ISSN: 1471003X. DOI: 10.1038/nrn1296.

[62] J. Krupic, M. Bauza, S. Burton, C. Barry, and J. O'Keefe. "Grid cell symmetry is shaped by environmental geometry." In: *Nature* (2015). ISSN: 14764687. DOI: 10.1038/nature14153.

[63] J. Krupic, M. Bauza, S. Burton, and J. O'Keefe. "Local transformations of the hippocampal cognitive map." In:

Science (2018). ISSN: 10959203. DOI: 10.1126/science. aao4960.

[64] R. F. Langston, J. A. Ainge, J. J. Couey, C. B. Canto, T. L. Bjerknes, M. P. Witter, E. I. Moser, and M. B. Moser. "Development of the spatial representation system in the rat." In: *Science* (2010). ISSN: 00368075. DOI: 10.1126/science.1188210.

[65] P. Latuske, O. Toader, and K. Allen. "Interspike intervals reveal functionally distinct cell populations in the medial entorhinal cortex." In: *Journal of Neuroscience* (2015). ISSN: 15292401. DOI: 10.1523/JNEUROSCI.0276-15.2015.

[66] H. J. Lenzen. *Die Brieftaube: Geschichte, Pflege und Dressur derselbenTitle*. Dresden: Meinhold & Söhne, Königliche Hofbuchdruckerei, 1873, p. 82.

[67] J. K. Leutgeb, S. Leutgeb, A. Tashiro, E. I. Moser, and M. B. Moser. "The encoding of novelty in the dentate gyrus and CA3 network." In: *Society for Neuroscience Meeting Abstracts* (2007).

[68] S. Leutgeb, J. K. Leutgeb, C. A. Barnes, E. I. Moser, B. L. Mc-Naughton, and M. B. Moser. "Neuroscience: Independent codes for spatial and episodic memory in hippocampal neuronal ensembles." In: *Science* (2005). ISSN: 00368075. DOI: 10.1126/science.1114037.

[69] F. T. Lewis. "The significance of the term Hippocampus." In: *Journal of Comparative Neurology* (1923). ISSN: 10969861. DOI: 10.1002/cne.900350303.

[70] P. A. Lipton, J. A. White, and H. Eichenbaum. "Disambiguation of overlapping experiences by neurons in the

medial entorhinal cortex." In: *Journal of Neuroscience* (2007). ISSN: 02706474. DOI: 10.1523/JNEUROSCI.1063-07.2007.

[71] J. E. Lisman. "Bursts as a unit of neural information: Making unreliable synapses reliable." In: *Trends in Neurosciences* (1997). ISSN: 01662236. DOI: 10.1016/S0166-2236(96)10070-9.

[72] J. R. Manns, M. W. Howard, and H. Eichenbaum. "Gradual Changes in Hippocampal Activity Support Remembering the Order of Events." In: *Neuron* (2007). ISSN: 08966273. DOI: 10.1016/j.neuron.2007.08.017.

[73] E. Marozzi, L. L. Ginzberg, A. Alenda, and K. J. Jeffery. "Purely translational realignment in grid cell firing patterns following nonmetric context change." In: *Cerebral Cortex* (2015). ISSN: 14602199. DOI: 10.1093/cercor/bhv120.

[74] A. Mathis, A. V. M. Herz, and M. Stemmler. "Optimal population codes for space: Grid cells outperform place cells." In: *Neural Computation* (2012). ISSN: 08997667. DOI: 10.1162/NECO_a_00319.

[75] T. Maudlin. *Philosophy of physics: Space and time*. 2012. ISBN: 9781400842339. DOI: 10.1080/10848770.2014.990269.

[76] B. L. McNaughton, F. P. Battaglia, O. Jensen, E. I. Moser, and M. B. Moser. "Path integration and the neural basis of the 'cognitive map'." In: *Nature Reviews Neuroscience* (2006). ISSN: 1471003X. DOI: 10.1038/nrn1932.

[77] J. F. Mitchell, K. A. Sundberg, and J. H. Reynolds. "Differential Attention-Dependent Response Modulation across Cell Classes in Macaque Visual Area V4." In: *Neuron* (2007). ISSN: 08966273. DOI: 10.1016/j.neuron.2007.06.018.

[78]   J. F. Mitchell, K. A. Sundberg, and J. H. Reynolds. "Spatial Attention Decorrelates Intrinsic Activity Fluctuations in Macaque Area V4." In: *Neuron* (2009). ISSN: 08966273. DOI: 10.1016/j.neuron.2009.09.013.

[79]   M.-L. Mittelstaedt and H. Mittelstaedt. "Homing by path integration in a mammal." In: *Naturwissenschaften* (1980). ISSN: 14321904. DOI: 10.1007/BF00450672.

[80]   S. J. Y. Mizumori and J. D. Williams. "Directionally selective mnemonic properties of neurons in the lateral dorsal nucleus of the thalamus of rats." In: *Journal of Neuroscience* (1993). ISSN: 02706474. DOI: 10.1523/jneurosci.13-09-04015.1993.

[81]   K. Mizuseki, K. Diba, E. Pastalkova, and G. Buzsáki. "Hippocampal CA1 pyramidal cells form functionally distinct sublayers." In: *Nature Neuroscience* (2011). ISSN: 10976256. DOI: 10.1038/nn.2894.

[82]   E. I. Moser and M. B. Moser. "A metric for space." In: *Hippocampus* (2008). ISSN: 10509631. DOI: 10.1002/hipo.20483.

[83]   E. I. Moser, M. B. Moser, and B. L. McNaughton. "Spatial representation in the hippocampal formation: A history." In: *Nature Neuroscience* (2017). ISSN: 15461726. DOI: 10.1038/nn.4653.

[84]   E. I. Moser, Y. Roudi, M. P. Witter, C. Kentros, T. Bonhoeffer, and M. B. Moser. "Grid cells and cortical representation." In: *Nature Reviews Neuroscience* (2014). ISSN: 14710048. DOI: 10.1038/nrn3766.

[85] R. U. Muller and J. L. Kubie. "The effects of changes in the environment on the spatial firing of hippocampal complex-spike cells." In: *Journal of Neuroscience* (1987). ISSN: 02706474. DOI: 10.1523/jneurosci.07-07-01951.1987.

[86] R. U. Muller, J. L. Kubie, and J. B. Ranck. "Spatial firing patterns of hippocampal complex-spike cells in a fixed environment." In: *Journal of Neuroscience* (1987). ISSN: 02706474. DOI: 10.1523/jneurosci.07-07-01935.1987.

[87] J. O'Keefe. "Place units in the hippocampus of the freely moving rat." In: *Experimental Neurology* (1976). ISSN: 10902430. DOI: 10.1016/0014-4886(76)90055-8.

[88] J. O'Keefe and J. Dostrovsky. "The hippocampus as a spatial map. Preliminary evidence from unit activity in the freely-moving rat." In: *Brain Research* (1971). ISSN: 00068993. DOI: 10.1016/0006-8993(71)90358-1.

[89] J. O'Keefe and L. Nadel. *The Hippocampus as a cognitive map*. Oxford: Oxford University Press, 1978, p. 570. ISBN: 0-19-857206-9.

[90] J. O'Keefe and M. L. Recce. "Phase relationship between hippocampal place units and the EEG theta rhythm." In: *Hippocampus* (1993). ISSN: 10981063. DOI: 10.1002/hipo.450030307.

[91] T. Otto, H. Eichenbaum, C. G. Wible, and S. I. Wiener. "Learning-related patterns of CA1 spike trains parallel stimulation parameters optimal for inducing hippocampal long-term potentiation." In: *Hippocampus* (1991). ISSN: 10981063. DOI: 10.1002/hipo.450010206.

[92]   E. H. Park, D. Dvorak, and A. A. Fenton. "Ensemble place codes in hippocampus: CA1, CA3, and dentate gyrus place cells have multiple place fields in large environments." In: *PLoS ONE* (2011). ISSN: 19326203. DOI: 10.1371/journal.pone.0022349.

[93]   J. A. Pérez-Escobar, O. Kornienko, P. Latuske, L. Kohler, and K. Allen. "Visual landmarks sharpen grid cell metric and confer context specificity to neurons of the medial entorhinal cortex." In: *eLife* (2016). ISSN: 2050084X. DOI: 10.7554/eLife.16937.

[94]   M. Poth and A. V. M. Herz. "Burst activity plays no role for the field-to-field variability and rate remapping of grid cells." In: *bioRxiv* (2020). DOI: 10.1101/2020.03.28.013318.

[95]   M. Pröll, S. Häusler, and A. V. M. Herz. "Grid-cell activity on linear tracks indicates purely translational remapping of 2D firing patterns at movement turning points." In: *Journal of Neuroscience* 38.31 (2018), pp. 7004–7011. ISSN: 1529-2401. DOI: 10.1523/JNEUROSCI.0413-18.2018.

[96]   G. J. Quirk, R. U. Muller, J. L. Kubie, and J. B. Ranck. "The positional firing properties of medial entorhinal neurons: Description and comparison with hippocampal place cells." In: *Journal of Neuroscience* (1992). ISSN: 02706474. DOI: 10.1523/jneurosci.12-05-01945.1992.

[97]   A. D. Redish. *Beyond the Cognitive Map*. 1999. DOI: 10.7551/mitpress/1571.001.0001.

[98]   D. S. Reich, F. Mechler, K. P. Purpura, and J. D. Victor. "Interspike intervals, receptive fields, and information encoding in primary visual cortex." In: *Journal of Neuroscience*

(2000). ISSN: 02706474. DOI: 10.1523/jneurosci.20-05-01964.2000.

[99] E. T. Reifenstein, R. Kempter, S. Schreiber, M. B. Stemmler, and A. V. M. Herz. "Grid cells in rat entorhinal cortex encode physical space with independent firing fields and phase precession at the single-trial level." In: *Proceedings of the National Academy of Sciences of the United States of America* (2012). ISSN: 00278424. DOI: 10.1073/pnas.1109599109.

[100] E. Reifenstein, M. Stemmler, A. V. M. Herz, R. Kempter, and S. Schreiber. "Movement dependence and layer specificity of entorhinal phase precession in two-dimensional environments." In: *PLoS ONE* (2014). ISSN: 19326203. DOI: 10.1371/journal.pone.0100638.

[101] A. Renart and C. K. Machens. "Variability in neural activity and behavior." In: *Current Opinion in Neurobiology* (2014). ISSN: 18736882. DOI: 10.1016/j.conb.2014.02.013.

[102] H. Sanders, D. Ji, T. Sasaki, J. K. Leutgeb, M. A. Wilson, and J. E. Lisman. "Temporal coding and rate remapping: Representation of nonspatial information in the hippocampus." In: *Hippocampus* (2019). ISSN: 10981063. DOI: 10.1002/hipo.23020.

[103] F. Sargolini, M. Fyhn, T. Hafting, B. L. McNaughton, M. P. Witter, M. B. Moser, and E. I. Moser. "Conjunctive representation of position, direction, and velocity in entorhinal cortex." In: *Science* (2006). ISSN: 00368075. DOI: 10.1126/science.1125572.

[104] S. Sassi and R. Wehner. "Dead reckoning in desert ants Cataglyphis fortis: Can homeward-bound vectors be re-

activated by familiar landmark configuration?" In: *Proc Neurobiol Conf Göttingen* 25 (1997), p. 484.

[105]   F. Savelli, D. Yoganarasimha, and J. J. Knierim. "Influence of boundary removal on the spatial representations of the medial entorhinal cortex." In: *Hippocampus* (2008). ISSN: 10509631. DOI: 10.1002/hipo.20511.

[106]   S. Schreiber, I. Erchova, U. Heinemann, and A. V. M. Herz. "Subthreshold resonance explains the frequency-dependent integration of periodic as well as random stimuli in the entorhinal cortex." In: *Journal of Neurophysiology* (2004). ISSN: 00223077. DOI: 10.1152/jn.01116.2003.

[107]   H. Schubert. *TOPOLOGY*. Macdonald & Company, 1968, p. 358. ISBN: 0356020770, 9780356020778.

[108]   W. B. Scoville and B. Milner. "Loss of recent memory after bilateral hippocampal lesions." In: *Journal of neurology, neurosurgery, and psychiatry* (1957). ISSN: 00223050. DOI: 10.1136/jnnp.20.1.11.

[109]   J. Simonnet and M. Brecht. "Burst firing and spatial coding in subicular principal cells." In: *Journal of Neuroscience* (2019). ISSN: 15292401. DOI: 10.1523/JNEUROSCI.1656-18.2019.

[110]   R. K. Snider, J. F. Kabara, B. R. Roig, and A. B. Bonds. "Burst firing and modulation of functional connectivity in cat striate cortex." In: *Journal of Neurophysiology* (1998). ISSN: 00223077. DOI: 10.1152/jn.1998.80.2.730.

[111]   L. R. Squire. "Memory and the Hippocampuss: A Synthesis From Findings With Rats, Monkeys, and Humans." In: *Psychological Review* (1992). ISSN: 0033295X. DOI: 10.1037/0033-295X.99.2.195.

[112] M. Stemmler, A. Mathis, and A. V. M. Herz. "Neuroscience: Connecting multiple spatial scales to decode the population activity of grid cells." In: *Science Advances* (2015). ISSN: 23752548. DOI: 10.1126/science.1500816.

[113] H. Stensola, T. Stensola, T. Solstad, K. FrØland, M. B. Moser, and E. I. Moser. "The entorhinal grid map is discretized." In: *Nature* (2012). ISSN: 00280836. DOI: 10.1038/nature11649.

[114] T. Stensola, H. Stensola, M. B. Moser, and E. I. Moser. "Shearing-induced asymmetry in entorhinal grid cells." In: *Nature* (2015). ISSN: 14764687. DOI: 10.1038/nature14151.

[115] B. A. Strange, M. P. Witter, E. S. Lein, and E. I. Moser. "Functional organization of the hippocampal longitudinal axis." In: *Nature Reviews Neuroscience* (2014). ISSN: 14710048. DOI: 10.1038/nrn3785.

[116] L. P. Sugrue, G. S. Corrado, and W. T. Newsome. "Matching behavior and the representation of value in the parietal cortex." In: *Science* (2004). ISSN: 00368075. DOI: 10.1126/science.1094765.

[117] J. S. Taube. "Head direction cells recorded in the anterior thalamic nuclei of freely moving rats." In: *Journal of Neuroscience* (1995). ISSN: 02706474. DOI: 10.1523/jneurosci.15-01-00070.1995.

[118] J. S. Taube. "The Head Direction Signal: Origins and Sensory-Motor Integration." In: *Annual Review of Neuroscience* (2007). ISSN: 0147-006X. DOI: 10.1146/annurev.neuro.29.051605.112854.

[119] J. S. Taube, R. U. Muller, and J. B. Ranck. "Head-direction cells recorded from the postsubiculum in freely moving rats. I. Description and quantitative analysis." In: *Journal of Neuroscience* (1990). ISSN: 02706474. DOI: `10.1523/jneurosci.10-02-00420.1990`.

[120] F. Theunissen and J. P. Miller. "Temporal encoding in nervous systems: A rigorous definition." In: *Journal of Computational Neuroscience* (1995). ISSN: 09295313. DOI: `10.1007/BF00961885`.

[121] L. T. Thompson and P. J. Best. "Long-term stability of the place-field activity of single units recorded from the dorsal hippocampus of freely behaving rats." In: *Brain Research* (1990). ISSN: 00068993. DOI: `10.1016/0006-8993(90)90555-P`.

[122] S. J. Thorpe. "Spike arrival times: A highly efficient coding scheme for neural networks." In: *Parallel processing in neural systems* (1990), pp. 91–94.

[123] E. C. Tolman. "Cognitive maps in rats and men." In: *Psychological Review* (1948). ISSN: 0033295X. DOI: `10.1037/h0061626`.

[124] E. Tulving and H. J. Markowitsch. "Episodic and declarative memory: Role of the hippocampus." In: *Hippocampus* (1998). ISSN: 10509631. DOI: `10.1002/(SICI)1098-1063(1998)8:3<198::AID-HIPO2>3.0.CO;2-G`.

[125] F. Vargha-Khadem, D. G. Gadian, K. E. Watkins, A. Connelly, W. Van Paesschen, and M. Mishkin. "Differential effects of early hippocampal pathology on episodic and semantic memory." In: *Science* (1997). ISSN: 00368075. DOI: `10.1126/science.277.5324.376`.

[126]   R. Wehner. "Optische Orientierungsmechanismen im Heimkehr-Verhalten von Cataglyphis bicolor Fab. (Formicidae, Hymenoptera)." In: *Rev. Suisse Zool.* (1968).

[127]   X. X. Wei, J. Prentice, and V. Balasubramanian. "A principle of economy predicts the functional architecture of grid cells." In: *eLife* (2015). ISSN: 2050084X. DOI: 10.7554/eLife.08362.

[128]   T. J. Wills, F. Cacucci, N. Burgess, and J. O'Keefe. "Development of the hippocampal cognitive map in preweanling rats." In: *Science* (2010). ISSN: 00368075. DOI: 10.1126/science.1188224.

[129]   M. A. Wilson and B. L. McNaughton. "Dynamics of the hippocampal ensemble code for space." In: *Science* (1993). ISSN: 00368075. DOI: 10.1126/science.8351520.

[130]   R. M. Yoder and J. S. Taube. "The vestibular contribution to the head direction signal and navigation." In: *Frontiers in Integrative Neuroscience* (2014). ISSN: 16625145. DOI: 10.3389/fnint.2014.00032.

[131]   K. J. Yoon, S. Lewallen, A. A. Kinkhabwala, D. W. Tank, and I. R. Fiete. "Grid Cell Responses in 1D Environments Assessed as Slices through a 2D Lattice." In: *Neuron* (2016). ISSN: 10974199. DOI: 10.1016/j.neuron.2016.01.039.

[132]   F. Zeldenrust, W. J. Wadman, and B. Englitz. "Neural coding with bursts—Current state and future perspectives." In: *Frontiers in Computational Neuroscience* (2018). ISSN: 16625188. DOI: 10.3389/fncom.2018.00048.

ACKNOWLEDGMENTS

PUBLICATIONS

M. Pröll, S. Häusler, and A.V.M. Herz. "Grid-cell activity on linear tracks indicates purely translational remapping of 2D firing patterns at movement turning points." In: *Journal of Neuroscience* (2018), accepted June 24, 2018.

M. Poth and A.V.M. Herz. "Burst activity plays no role for the field-to-field variability and rate remapping of grid cells." submitted to *Hippocampus*, March 29, 2020.

AFFIDAVIT

Eidesstattliche Versicherung/Affidavit

Hiermit versichere ich an Eides statt, dass ich die vorliegende Dissertation selbstständig angefertigt habe, mich außer der angegebenen keiner weiteren Hilfsmittel bedient und alle Erkenntnisse, die aus dem Schrifttum ganz oder annähernd übernommen sind, als solche kenntlich gemacht und nach ihrer Herkunft unter Bezeichnung der Fundstelle einzeln nachgewiesen habe.

I hereby confirm that the dissertation is the result of my own work and that I have only used sources or materials listed and specified in the dissertation.

Martinsried-Planegg, 03. April 2020

Michaela Poth (nee Pröll)

Michaela Poth (nee Pröll)

Prof. Dr. Andreas Herz